5-2017

An Electrochemical Characterization of a Vanadium-based Deoxydehydration Catalyst

Joel Eric Baker
University of Arkansas, Fayetteville

An Electrochemical Characterization of a Vanadium-based Deoxydehydration Catalyst

A thesis submitted in partial fulfillment
of the requirements for the degree of
Master of Science in Chemistry

by

Joel E. Baker
Missouri Southern State University
Bachelor of Science in Chemistry, 2014

May 2017
University of Arkansas

This thesis is approved for recommendation to the Graduate Council.

_____
Dr. Stefan Kilyanek
Thesis Director

_____
Dr. David Paul
Committee Member

_____
Dr. Ryan Tian
Committee Member

_____
Dr. Bill Durham
Committee Membe

Abstract

Alternative methods for the conversion of polyols into olefins, be it for carbon storage or hydrocarbon fuel production, have become prevalent in today's chemical industry. One process in particular, deoxydehydration (DODH) has been proven effective in taking sustainable biomass derivatives and converting them through the utilization of various homogenous metal catalysts. While this process may show productive yields and material conversion, it is hindered by the need of a sacrificial reductant. This makes a novel process economically unviable and relatively unused outside of scientific research. That fact begs the question: Can the process be improved? It is proposed here that DODH catalysis and similar processes can be made more practical through the elimination of a sacrificial reductant and the utilization of a vanadium-centered proton coupled electron transfer (PCET). For this to be realized a known DODH catalyst, [tetrabutylammonium][dioxovanadium(V)2,6-pyridinedicarboxylate] (TBADVP), must first be characterized electrochemically.

Acknowledgements

A special thanks to my advisor Dr. Stefan Kilyanek for guiding me through my time here at the University of Arkansas and for all of the support that he has shown me through good times and bad.

Also, thank you to my committee members for the knowledge they instilled upon me through these few years. I am wholeheartedly grateful for all of the indispensable things that I have learned during my time here.

Dedication

This is for my family; I could have not done any of this without them.

Table of Contents

I. Introduction

In today's society the public is surrounded by numerous volatile markets. These markets not only influence our pocketbooks but also our collective, moral conscience. There's one market that faces daily scrutiny and that is the fossil fuels market, specifically petroleum. Almost everything a person comes in contact with is directly related to petroleum and petroleum derivatives in one way or another. Be it the plastic cup that holds a child's drinking water or the shoes on athlete's feet none of it would be possible without current petroleum infrastructure. The largest form of oil consumption nationally (and worldwide) is gasoline. As a nation the United States consumes ~20% of the world production of petroleum, 47% of which is gasoline. The other 53% is a combination of distillate fuel, gas liquids, kerosene, still gas, plastics, lubricants, and the list goes on. [15] Consumption of oil reserves is a building concern in today's society as well as the environmental impact of extraction, refining, transportation, and consumption of petroleum products. While there is a debate about the impact the release of greenhouse gases (such as CO_2) have on the environment the foot print still exists. CO_2 emissions in the United States alone totaled 5.15 billion tons in 2015 (with a 5% uncertainty, this included all aspects of CO_2 release such as industry, transportation, mining, and environmental impacts such as oil spills). [16] It is important that alternative pathways be found to replace petroleum based fuels and materials to offset the ever increasing economic and environmental impacts being experienced today. One path in particular, the conversion of biomass into olefins, has the potential to reduce the impacts caused by petroleum and fossil fuels. Olefins, specifically C_2 to C_4, are the feed stocks for the chemical industry. While typically supplied through the fractionation of crude oil, these simple components can be made from a sustainable resource: biomass. Biomass is already abundant and can come in several forms; directly grown and supplied or recycled from remainder waste such

as corn stover and logging scrap. Step one is to take biomass and convert it through fermentation, gasification, or dehydrogenation to provide bio-intermediates that can then be transformed into bio-olefins through various chemical processes. [17][23] Deoxydehydration (**DODH**) is one such process that has shown extremely efficient conversion and yield results when assisted by homogeneous metal-oxo catalysts. [1] The process is hindered by the need for sacrificial reductants making olefin conversion potentially toxic, costly, and inconvenient. It is the goal of this research to take a metal-oxo catalyst capable of **DODH** [tetrabutylammonium][dioxovanadium(V)2,6-pyridinedicarboxylate] (**TBADVP**) and electrochemically characterizing it and show that **DODH** can be performed in the presence of only catalyst, polyols, and acidic protons.

II. Background

A. Deoxydehydration

The process of **DODH** using transition metal catalysts was first reported by Cook and Andrews in 1996 using a Rhenium metal-oxo catalyst, $(C_5Me_5)ReO_3$. The catalytic cycle, ran in chlorobenzene, featured a Re^{VII}/Re^{V} couple and a triphenylphosphine (**TPP**) mediated oxygen abstraction to transform a diol into an alkene and water. [10] The **DODH** catalytic process in question, designed by Nicolas, et al. in 2013, is analogous to the Cook/Andrew method with its use of a metal-oxo catalyst and sacrificial oxygen abstraction reductant. The **DODH** catalyst, **TBADVP**, starts with glycol condensation, which is followed by oxygen abstraction using either **TPP** or sodium sulfite, and then finishes with an oxidative elimination to yield an olefin product and a regenerated metal-oxo catalyst. An alternative route being oxygen abstraction, condensation, and then olefin extrusion; see "Scheme (1)" below. [1] More recently, the Nicolas

group has found that hydrogen and carbon monoxide may also be used in the catalytic cycle as sacrificial reductants. [2] Experimental conditions for the **TBADVP** catalyst: benzene solvent and **TPP** reductant, conducted at 150-170 °C in either a thick-walled glass tube or stainless steel reactor. The experiment was allowed to run until completion (72 hours) to give one hundred percent conversion and an olefin yield of 95% [1] The vanadium V/III couple seen in the Nicolas **DODH** is of interest and is the focus of the work herein.

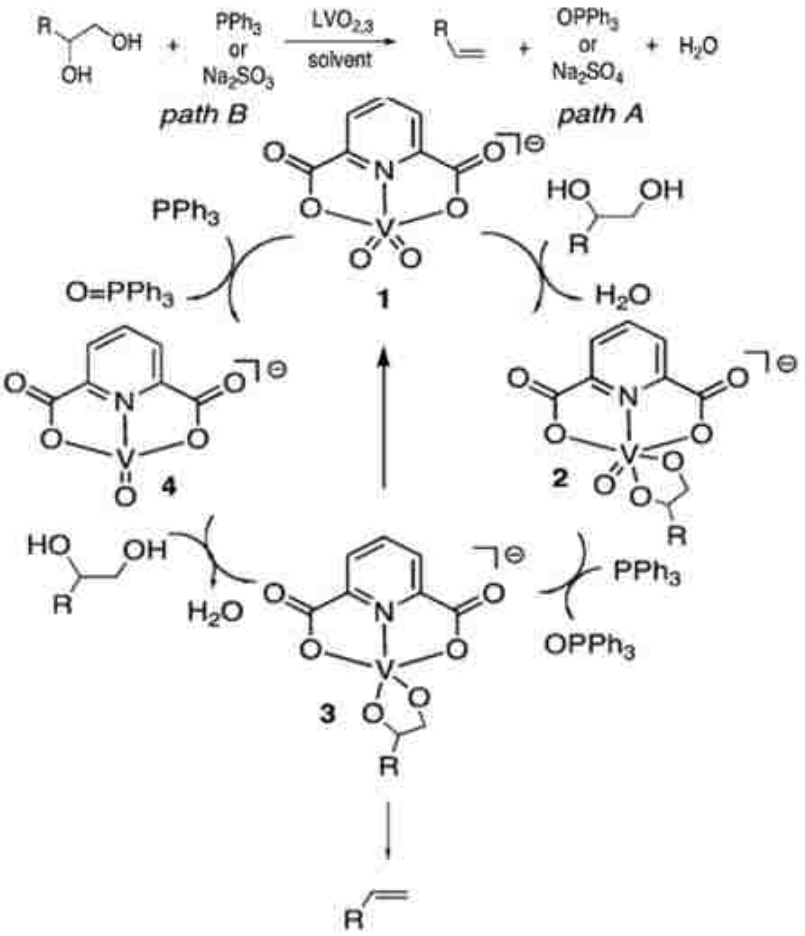

"Scheme (1) Putative catalytic cycle for DODH catalyzed by TBADVP." Figure taken from page 8200, Chapman, G.; Nicholas, K. M. Vanadium-catalyzed deoxydehydration of glycols. *Chem. Comm.* 2013, *49*, 8199-8201.

B. Proton Coupled Electron Transfer

Proton coupled electron transfer (**PCET)** reactions surround us in our everyday lives: Photosystem II, enzyme systems such as DNA photolayse, and photocatalytic water splitting all rely on **PCET** pathways. While these systems have been thoroughly studied in the past the relationship **PCET** plays has yet to be fully understood. **PCET** is exactly what it sounds like, the transfer and addition of both a proton and an electron to a compound either one at a time (step-wise) or at the same time (concerted proton electron transfer, **CPET**). In the case of metal-oxo species being reduced to a metal-hydroxo the overall process can be described as a hydrogen atom transfer (**HAT**), which is analogous to a **CPET** of $1H^+/1e^-$. An additional term of "hydride transfer" may be used which describes the transfer of a single proton and two electrons in the form of H^-. [4] The **TBADVP** species is believed to undergo **PCET** in a manner similar to **HAT**. While it may appear that a step-wise electron transfer would be preferred, a concerted path is thermodynamically favored due to the step-wise intermediate being uphill in energy while the final product is of a lower energy. [5] The mechanism of **PCET** has been suggested to involve an outer sphere electron transfer based on redox kinetics but in the case of electrochemical analysis it is understood that it is a **CPET** of the inner sphere variety. This would require a heterogeneous component (electrode surface, e^- source), a solvated component (H^+ source), and the transfer species to be coordinated before the transfer of both electron and proton may occur. Stepwise and concerted transfers can appear the same in some studies and can only be delineated through the study of reaction kinetics. Electrochemical analysis is the most popular technique to observe **PCET** but it can also be observed through indirect electrochemical analysis or photo induction/quenching techniques. [3]

C. Electrochemical Analysis

Cyclic Voltammetry: The Nernst Equation and the Pourbaix Diagram

Cyclic Voltammetry is one of the most common electrochemical analyses that can be performed on a chemical compound in solution. The electrochemical cell experiences an induced potential that is then swept over a chosen potential range. The resulting current at each potential step is then recorded to give a plot of current (i, Amperes) versus potential (V, Volts). As the applied potential is scanned cathodically from open circuit, a species in solution may undergo an electrochemical reduction. The potential sweep may then be "turned around" and swept anodically allowing a solution species to be electrochemically oxidized to reveal a redox couple. The shape of the current-potential plot can reveal useful preliminary information about the molecular processes that are occurring in the electrochemical cell at the electrode surface. A Nernstian, one-electron redox wave will display a cyclic voltammogram, (**CV**) in which both the forward and backward scans are superimposable (having equal currents) and have a peak potential separation (ΔE_p) of 59.06 mV (equal to $\frac{2.3RT}{nF}$ in Equation 1). In the case where the reducible species does not show appreciable interaction upon oxidation a superimposable **CV** with reversible 1e- dynamics is seen but with a peak potential separation of approximately 35.6mV hinting at the combination of two separate 1e- transfers that occur at the same potential. Some step-wise 2e- redox couples will appear as two distinct reversible waves each with ΔE_p = 59.06mV (Equation 2) or as staggered waves that overlap with $\Delta E_p > 120$ mV. In cases where reversible behavior is seen but $\Delta E_p > 59.06$mV it is possible the electron transfer may be reversible but sluggish in nature, not exhibiting fast electron transfer kinetics. [6]

(1) (Nernst Equation): $E_e = E^0 + \frac{2.3RT}{nF} log \frac{[reduced]}{[oxidized]}$

(n= number of electrons transferred)

(2): $E_k^0 - E_1^0 = -\left(\frac{2.3RT}{F}\right) \ln k$

(k=2 [electrons])

Electron transfers can be evaluated further by varying the pH (donator-acceptor ratio) of the cell solution and observing a redox couple under constant experimental conditions. Plotting potential (E^0) versus pH will give a Pourbaix diagram. In a system involving a solid (the electrode surface), a dissolved substance (homogenous catalyst), free electrons (applied potential), and hydrogen ions (acidic media) a Pourbaix diagram with a slope equal to $-\frac{0.05906*h}{n}$ will be generated (n= number of electrons transferred, h=number of protons transferred, similar to the term seen in the Nernst equation above). [7] A slope of ~0.060V is indicative of systems with equal ratio of electrons and protons. While ~0.030V implies two electrons and one proton, ~0.039V three electrons and two proton, and ~0.044V would imply the transfer of four electrons and three protons.

Electrode Kinetics and Tafel/Butler-Volmer Equations

The current of an electrochemical system is dependent on the ability of solution reactants to be transported to and from the electrode surface. This depends on interfacial dynamics rather than interfacial kinetics. In cases of solution stirring, or electrode rotation, mass-transport has little to no effect on the resulting electrode currents. The Tafel Equation (Equation 3) has shown that such current is exponentially related to the overpotential applied to the system. [6]

$$(3): i = a' * e^{\frac{\eta}{b'}}$$

(Analogous to $\eta = a + b \log i$)

If a reaction has both a forward and backward path,

$$O + ne \overset{k_f}{\rightarrow} R \; likewise \; R \overset{k_b}{\rightarrow} O + ne$$

The reaction rates v_f / v_b can be expressed as:

$$(4): v_f = k_f C_O(0,t) = \frac{i_c}{nFA} \text{ and } v_b = k_b C_R(0,t) = \frac{i_c}{nFA}$$

Taking the difference of both the forward and backward reaction rates yields:

$$(5): v_{net} = v_f - v_b = k_f C_O(0,t) - k_b C_R(0,t) = \frac{i}{nFA}$$

Solving for i yields the overall form of:

$$(6): i = i_c - i_a = nFA[k_f C_O(0,t) - k_b C_R(0,t)]$$

Heterogeneous electrode kinetics must be expressed as cm/s as long as the concentration of substrate is expressed as mol/cm^3. It must be noted that the kinetic rate is expressed as the concentration of substrate at the electrode surface which may not necessarily be the same as the substrate concentration in the bulk solution. [6]

Consider a simple one-step one electron process, where the same forward and backward redox path applies, and assume that the system is at equilibrium. In a state of equilibrium the forward and backward reaction rates are of equal values. If we take the equilibrium potential as the new reference potential, rather than the potential at a reference electrode, the anode and cathode reactions can be expressed as reaction coordinates much like Marcus Theory. If the potential is lowered by an amount ΔE the new relative energy of an electron at the electrode surface then changes a quantity: $-F\Delta E = -F(E-E^0)$ lowering the energy of the $O + e^-$ curve in Figure (1),

effectively lowering the energy barrier for the oxidation of species R ($\Delta G_{0a}^{\neq}$).[6] This lowering in anodic energy is equal to:

$$(7): \Delta G_a^{\neq} = \Delta G_{0a}^{\neq} - (1-\alpha)F(E - E^{0`})$$

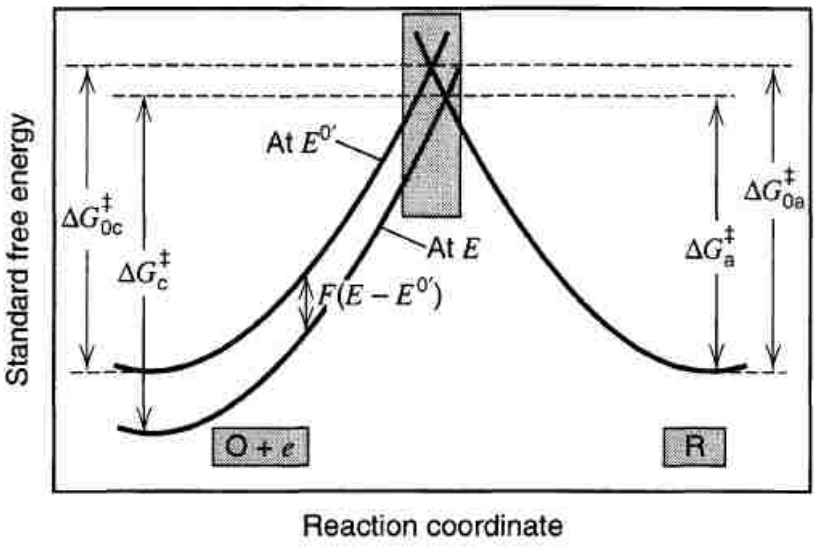

Figure 1: Effects of potential on standard free energies. Figure taken from page 95: Bard, A. L.; Faulkner, L. R. Electrochemical Methods: Fundamentals and Applications; Wiley: New York, 1980.

The lowering in cathodic energy can also be expressed in the same manner:

$$(8): \Delta G_c^{\neq} = \Delta G_{0c}^{\neq} + \alpha F(E - E^{0`})$$

Expressing the rates k_f and k_b in an Arrhenius form yields:

$$(9): k_f = A_f exp\left(-\frac{\Delta G_c^{\neq}}{RT}\right) \qquad (10): k_b = A_b exp\left(-\frac{\Delta G_a^{\neq}}{RT}\right)$$

Where substitution of (7) and (8) into (9) and (10) gives

$$(11): k_f = A_f exp\left(-\frac{\Delta G_{0c}^{\neq}}{RT}\right) \exp\left(\frac{-\alpha F(E-E^{0`})}{RT}\right) \quad (12): k_b = A_b exp\left(-\frac{\Delta G_{0a}^{\neq}}{RT}\right) exp\left(\frac{(1-\alpha)F(E-E^{0`})}{RT}\right)$$

In a situation where the concentration of both O in R in the bulk is equal then ($E = E^{0`}$) and ($k_f = k_b$). Under these conditions the standard rate constant k^0 can be used making equations (11) and (12):

$$(13): k_f = k^0 exp\left(\frac{-\alpha F(E-E^{0`})}{RT}\right) \qquad (14): k_b = k^0 exp\left(\frac{(1-\alpha)F(E-E^{0`})}{RT}\right)$$

Substitution of (13) and (14) into (6) gives the current-potential characteristic, better known as the Butler-Volmer kinetic expression [6]:

$$(15): i = FAk^0\left(C_O(0,t)e^{\frac{-\alpha F(E-E^{0`})}{RT}} - C_R(0,t)e^{\frac{(1-\alpha)F(E-E^{0`})}{RT}}\right)$$

If a solution is stirred at an appreciable rate (or the current is low enough to keep the substrate concentration difference at the electrode surface and the bulk negligible) the system can then be represented by the Butler-Volmer Equation:

$$(16): i = i_0\left[e^{-\propto f\eta} - e^{(1-\alpha)f\eta}\right]$$

A Tafel analysis involves plotting the log of current in the form of current density (log j) and plotting it against the overpotential, η. The slope of a Tafel plot will lead to two kinetic parameters; the slope allows for the calculation of the reaction transfer coefficient (α) (Equations 17a, 17b) and the intercept of the line will equal the exchange current (i_0, or exchange current density, j_0). Since back reactions cannot be assumed as negligible, both the cathodic and anodic lines diverge from linearity as η approaches zero. Both linear-like representations will also be influenced by mass transfer at large overpotentials causing them to deviate further. [6]

$$(17a)\ anodic\ slope = \frac{(1-\alpha)F}{2.3RT} \qquad (17b)\ cathodic\ slope = \frac{-\alpha F}{2.3RT}$$

Chronoamperometry, Linear Sweep Voltammetery, and Koutecky-Levich Analysis

Chronoamperometry (**CA**) and linear sweep voltammetry (**LSV**) are similar to **CV** in that a potential is applied to the electrochemical cell and the resulting current is measured. The difference in **CA** and **LSV** is that the working electrode is represented by a rotating-disk electrode (**RDE**). In **CA** the **RDE** has a particular over-potential applied, usually one that is slightly past the reduction or oxidation potential of the electrochemical species. Alternatively, in **LSV** the potential is scanned through a set voltage window. The **RDE** is then rotated at various rates while the applied potential is held constant (or scanned); the rotation allows laminar flow to allow a greater concentration of the electrochemical species to react at the electrode surface. This increase in reactivity is due to a decrease in the mass-transport effect. As mass-transport becomes negligible the electrode rotation reaches its effective limitation and diffusion-limited current (i_{dl}) is achieved. A plot of inverse diffusion-limited current density (j_{dl}^{-1}) versus the inverse square root of rotation rate ($\omega^{-1/2}$) yields a Koutecky-Levich (**KL**) plot. The **KL**-slope can be used to determine the number of electrons (n) being transferred and the **KL**-intercept assists in the calculation of the kinetic-limiting current (j_K) by using the following **KL** equations: [9]

$$(18)\ \frac{1}{j} = \frac{1}{j_L} + \frac{1}{j_K} = \frac{1}{(0.62nFAD^{2/3}\omega^{1/2}v^{-1/6})} + \frac{1}{j_K}$$

$$(19)\ slope = 0.62nFC_0{D_0}^{3/2}v^{-1/6}$$

$$(20)\ j_K = nFk^0C_0$$

Where jK/jL are the kinetic-/diffusion- limiting current densities (mA/cm^2), ω is the angular velocity of the rotating disk ($\omega = 2\pi f/60$, f is the linear rotating speed in rpm), n is the overall

number of electrons transferred in the redox process, F is the Faraday constant, C_0 is the redox species bulk concentration, D_O is the diffusion coefficient of the electro-active species, ν is the kinematic viscosity of the electrolyte solution, and k^0 is the electron transfer rate constant.

Differential Pulse Voltammetry

Differential pulse voltammetry (**DPV**) is a controlled-potential method in which pulse modulation programming is utilized to extract the faradaic current response from an electrochemical system. The waveform of **DPV** resembles that of staircase voltammetry with a staggered pulse pattern. [6] The current is first sampled after an initial resting period of time (τ′) and is followed by a potential pulse (ΔE) that is allowed to rest a period of time (τ) at the end of which the current is sampled a second time. The difference of the two current responses ($\delta i = i(\tau) - i(\tau')$) is then taken and recorded against base potential. The potential is then stepped forward a set increment and another pulse modulation occurs until a predetermined number of increments have passed.

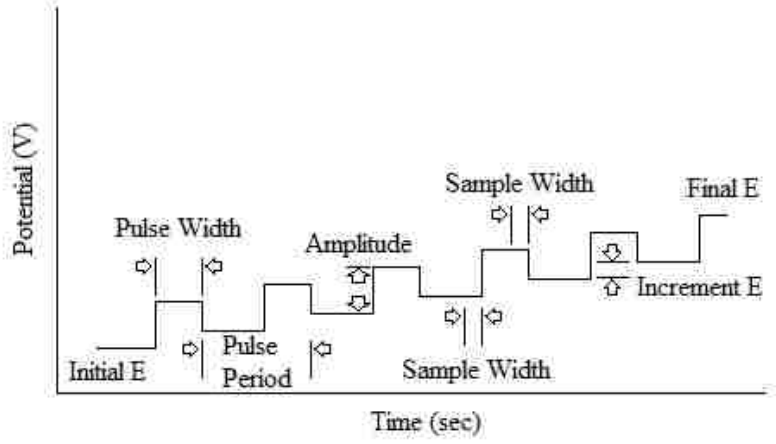

Figure 2: The differential pulse voltammetry wavefrom.

The resulting bell-shaped polarogram is a representation of peak current output and is governed by equation (21) [6] [12]:

$$(21)\ i_p = \left(\frac{nFAD^{1/2}C}{\pi^{1/2}(\tau-\tau')^{1/2}}\right)\cdot\left(\frac{1-\sigma}{1+\sigma}\right)\ where\ \sigma = exp\left(\frac{nF\Delta E}{2RT}\right)$$

Full width at half maximum of the corresponding peak can be used to determine the number of electrons transferred in some electrochemical systems when ΔE is less than 10 mV through the use of equation (22) [6] [12]:

$$(22)\ W_{1/2} = \frac{3.52RT}{nF}$$

$W_{1/2}$ will equal 90.4 for a one electron transfer and subsequently: 45.2 (n=2), 30.1 (n=3), and 22.6 (n=4). **DPV** is sensitive technique to provide detection limits as low as 5 x 10^{-8} M and can distinguish electro active components of homogeneous mixtures. [12] And while it was originally developed for the dropping mercury electrode it is a viable for use with stationary electrodes such as planar platinum and glassy carbon. [6]

Electrochemical Time of Flight (**ETOF**)

Diffusion of an electrochemical species can be measured through the use of an electrode array that consists of alternating generation electrodes and corresponding collection electrodes separated by a gap of measurable distance. Once a potential is applied the species being observed undergoes an electron transfer and then immediately diffuses away from the electrode surface. This diffusion then carries the electrochemically generated species to the collector electrode where it is immediately reduced or oxidized. This reduction/oxidation event can be measured by observing the response signal and determining the amount of time between complete generation

and collection. A typical response can be seen in Figure 3 showing the **ETOF** generation and collection of ferricyanide. [26a-26c]

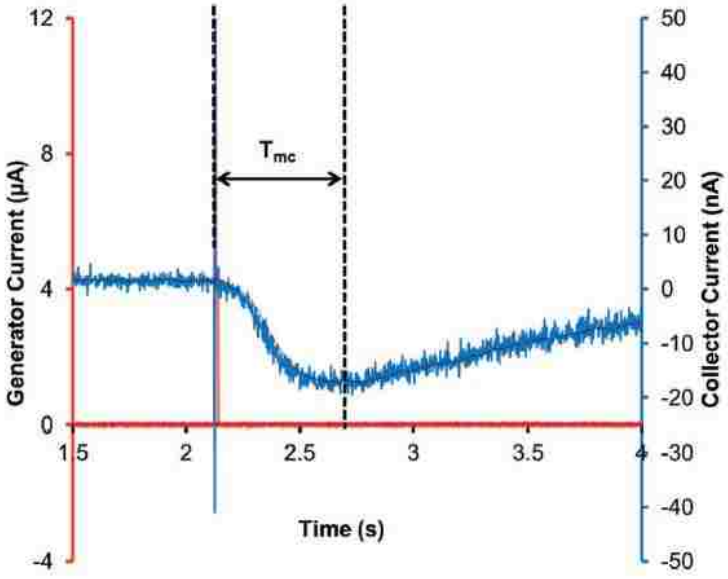

Figure 3: an example ETOF response of the electrochemical reduction (red cureve) and oxidation (blue curve) of ferricyanide. Figure taken from H673, Paul, D., Meier, M., Moldenhauer, J. Rapid and Direct Determination of Diffusion Coefficients Using Microelectrode Arrays. *J. Electrochem. Soc.* 2016, 163, (8), H672-H678.

This time is then compared to the distance traveled, typically micrometers, to calculate the diffusion coefficient of the generated species (Equation 23).

$$(23)\ d = K\sqrt{Dt_{mc}}$$

The distance travelled (d) between the generator and the edge of the collector is proportional to the geometric constant for the electrode array (K) multiplied by the square root of the diffusion coefficient for the species (**D**) times the time of maximum collection t_{mc}. Since this is the measurement of response only it is a concentration independent technique making it a useful tool for experimental comparison. Typical diffusion coefficient measurements fall within 10% of published values with a 95% confidence interval. [26a-26c]

III. Synthesis of Catalyst and Conjugate Salts

[Tetrabutylammonium][dioxovanadium(V) 2,6-pyridinedicarboxylate]

[n-Bu_4N]OH - A 0.4 M solution was prepared by diluting 100 mL of [n-Bu_4N]OH (40% wt. in H_2O, Aldrich) to 1 liter with deionized water.

[n-Bu_4N][VO_3] - Approximately 4.0 g of solid V_2O_5 (≥98%, Aldrich) was added to 200 mL 0.4M [n-Bu_4N]OH in a 500 mL Erlenmeyer flask and left to stir for approximately 18 hours at room temperature. The solution changed from a transparent yellow to nearly colorless liquid with a very small amount of colorless solid floating on the top. The solid was vacuum-filtered from the solution using a Buchner funnel and the remaining filtrate loaded into a 250mL round bottom flask. The filtrate was then dried on a rotary evaporator for 1-2 hours at 46° C until the appearance of viscous, light-brown oil. The round bottom flask was placed on a Schlenk line and left overnight to evaporate to complete dryness, yielding a crude, white solid. The flask was then back-filled with nitrogen, sealed, and transferred to a glovebox under a nitrogen atmosphere for extraction of the air-sensitive intermediate. 14 g of solid [n-Bu_4N][VO_3] were obtained (93% yield, 15.089 g Theoretical Yield). [8]

[n-Bu_4N][(pyridine-2,6-dicarboxylate)VO_2] - Approximately 1 gram [n-Bu_4N][VO_3], 0.5 g 2,6-pyridine dicarboxylic acid (99%, Aldrich), and 3g 4 Å molecular sieves were placed in 15-20mL dichloromethane (99.8%, anhydrous, Sigma-Aldrich) and left to stir for ~45 minutes. The sieves and insoluble solid were vacuum-filtered using a fritted funnel and flask. The remaining filtrate was then pumped down to ~4 mL, layered with diethyl ether (dried, Sigma-Aldrich), and placed in the glovebox freezer for crystallization. After seven days the mother liquor was decanted and

the wet crystals dried under vacuum. The crystalline solid was then transferred to a clean vial, triturated with fresh diethyl ether, dried again under vacuum and then weighed. Typical final product yield: 0.88-0.92 g. [1] A ^{1}HNMR spectrum can be found in the Appendix.

[n-Bu_4N][dichloroacetate]

Synthesis adapted from procedures found in references 21 and 22. Equimolar amounts of dichloroacetic acid (3.198 mL, 1.563 g/mL, 128.94 g/mol., 5.0 g, 0.0388 mol., ≥ 99%, Sigma-Aldrich) and 0.4M [n-Bu_4N]OH (0.097 L, 0.0388 mol.) were placed in a round bottom flask and left to stir for approximately 90 minutes. Once fully dissolved the clear solution was gravity filtered through filter paper to remove any traces of unreacted solid and the mixing stir bar. The filtered solution was then dried on a rotovap yielding an oily white solid. The oil was then allowed to crystallize overnight at -5.0 °C. The white solid was placed on the rotovap a second time and dried yielding a white solid. 11.82 g of white solid were produced. The white solid was then moved to a nitrogen atmosphere and dissolved in 15 mL dichloromethane and further dried under 5 g of 4Å sieves. The solution was then filtered via glass frit and dried under vacuum resulting in 7.58 g of light brown crystalline solid; a yield of 53% (14.35 g theoretical yield). A ^{1}HNMR spectrum can be found in the Appendix.

[n-Bu_4N][trichloroacetate]

Synthesis adapted from procedures found in references 21 and 22. Equimolar amounts of dichloroacetic acid (7.857 mL, 1.62 g/mL, 163.9 g/mol., 4.85 g, 0.0296 mol., ≥ 99.9%, Sigma-Aldrich) and 0.4M [n-Bu_4N]OH (0.074 L, 0.0296 mol., Aldrich) were placed in a round bottom flask and left to stir for approximately 90 minutes. Once fully dissolved the clear solution was gravity filtered through filter paper to remove any traces of unreacted solid and the mixing stir bar. The filtered solution was then dried on a rotovap yielding an oily white solid. The oil was then allowed to crystallize overnight at -5.0 °C. The white solid was placed on the rotovap a second time and dried yielding a white solid. 5.962 g of white solid were produced. Several grams were lost due to bump loss and were not recovered. The white solid was then moved to a nitrogen atmosphere and dissolved in 15 mL dichloromethane and further dried under 5 g of 4Å sieves. The DCM solution was then filtered via glass frit and dried under vacuum resulting in 2.8 g of white crystalline solid; a yield of 23% (12.03 g theoretical yield). A ^{1}HNMR spectrum can be found in the Appendix.

[n-Bu_4N][3,4-dichlorbenzoate]

Synthesis adapted from procedures found in references 21 and 22. Equimolar amounts of 3,4-dichorobenzoic acid (191.012 g/mol., 2.3972 g, 0.01255 mol., 99%, Aldrich) and 0.4M [n-Bu_4N]OH (0.097 L, 0.0128 mol., Aldrich) were placed in a round bottom flask and left to stir for approximately 90 minues. Once fully dissolved the clear solution was gravity filtered through filter paper to remove any traces of unreacted solid and the mixing stir bar. The filtered solution was then dried on a rotovap yielding viscous rose colored oil. The oil was then allowed to

crystallize overnight at room temperature. 4.244 g of pink solid was produced for a final yield of 78% (5.453 g theoretical yield). A ^{1}HNMR spectrum can be found in the Appendix.

[n-Bu_4N][2,4-dichlorbenzoate]

Synthesis adapted from procedures found in references 21 and 22. Equimolar amounts of 2,4-dichorobenzoic acid (191.012 g/mol., 2.559 g, 0.0134 mol., 98%, Aldrich) and 0.4M [n-Bu_4N]OH (0.034 L, 0.0136 mol., Aldrich) were placed in a round bottom flask and left to stir for approximately 90 minutes. Once fully dissolved the clear solution was gravity filtered through filter paper to remove any traces of unreacted solid and the mixing stir bar. The filtered solution was then dried on a rotovap yielding viscous yellow colored oil. The oil was then allowed to crystallize overnight at room temperature. 5.16 g of white solid was produced for a final yield of 89% (5.795 g theoretical yield). A ^{1}HNMR spectrum can be found in the Appendix.

[n-Bu_4N][benzoate]

Synthesis adapted from procedures found in references 21 and 22. Equimolar amounts of benzoic acid (122.12 g/mol., 2.4424 g, 0.02 mol., ≥ 99.5%, Sigma-Aldrich) and 0.4M [n-Bu_4N]OH (0.050 L, 0.02 mol., Aldrich) were placed in a round bottom flask and left to stir for approximately 60 minutes. Once fully dissolved the clear solution was gravity filtered through filter paper to remove any traces of unreacted solid and the mixing stir bar. The filtered solution was then dried on a rotovap yielding milky viscous white colored oil. The flask of oil was placed in the freezer at -5 °C until thickened and then dried on the rotovap again at 70 °C. The oil was then poured into a scintillation vial and allowed to crystallize at room temperature. 6.04 g of

white solid was produced for a final yield of 83% (7.272 g theoretical yield). A ^{1}HNMR spectrum can be found in the Appendix.

[2,6-dichloroanilinium][PF_6]

Synthesis adapted from procedures found in references 18 and 20. 11.91g of 2,6-dichloroaniline (≥ 98%, Aldrich) was purified through sublimation at 150-175 °C to yield a fine white crystalline solid. 10.95 g pure product was recovered (92% yield). 4.11g (1062.02 g/mol., 0.0254 mol.) of pure product 22 mL diethyl ether (anhydrous, Sigma Aldrich) were then placed in a round bottom flask and stirred for approximately 5 minutes to ensure that all of the aniline species was dissolved. 3.9 mL (1.651 g/mL, 145.97 g/mol., 6.428 g, 0.0242 mol.) hexafluorophosphoric acid (55 wt% H_2O, Aldrich) was then added drop-wise to the mixture (to avoid boiling of the ether) and then allowed to stir for 30 minutes. A white crystalline solid immediately precipitated. The diethyl ether was removed via rotovap giving approximately 6 g of product (80% yield, 7.45 g theoretical yield). [18a-18f] A ^{1}HNMR spectrum can be found in the Appendix.

[4-cyanoanilinium][PF_6]

Synthesis adapted from procedures found in references 18 and 20. 6.462 g (118.14 g/mol., 0.0547 mol.) of 4-aminobenzonitrile (98%, Sigma Aldrich) and 30 mL diethyl ether (anhydrous, Sigma Aldrich) were placed in a round bottom flask and stirred for approximately 15 minutes to ensure that all of the aniline species was dissolved. 7.64 mL (1.651 g/mL, 145.97 g/mol., 7.585 g, 0.05196 mol.) hexafluorophosphoric acid (55 wt% H_2O, Aldrich) was then added drop-wise to the mixture to avoid boiling of the ether and then allowed to stir for 90 minutes. A white crystalline solid immediately precipitated. The diethyl ether was removed via rotovap giving

approximately 6 g of white and yellow mixed product (50% yield, 12.651 g theoretical yield). The yellow impurity was then removed by dissolving the crude material in 100 mL acetonitrile (anhydrous, Sigma Aldrich) and reclaiming with diethyl ether (anhydrous, Sigma Aldrich). This process was repeated on additional time and the product dried via rotovap to yield a white crystalline solid. (5.9 g, 98% yield). [18] A ^{1}HNMR spectrum can be found in the Appendix.

IV. Electrochemistry Components

Electrochemical Setup

All electrochemistry performed occurs in a nitrogen-rich atmosphere using a custom, 4-probe electrochemical cell. The cell consists of a fritted counter compartment containing a platinum wire/mesh counter electrode (99.9999%, Alfa Aesar), non-aqueous silver/silver-cryptand reference electrode (BASi), and a working electrode. The working electrodes include gold, platinum, and glassy carbon materials either of the standard post variety (BASi) or quick change (rotating disk electrode, **RDE**) button variety (Pine Instruments). The **RDE** was controlled using a Metrohm Autolab RRDE. Data collection was done using a CH Instruments CH760E general purpose galvanostat and packaged CHI760E computer software. All data was processed using OriginPro and Microsoft Excel software. All experiments utilize a tetrabutylammonium hexafluorophosphate (**$TBAPF_6$**) electrolyte (electrochemical grade, ≥99%, Fluka) and acetonitrile solvent (anhydrous, 99.8%, Sigma-Aldrich) unless stated otherwise.

Silver Cryptand Reference Electrode

The silver/silver-cryptand reference was assembled using a kit purchased from Bioanalytical Systems, Inc. The electrode containment contains a silver wire, an acetonitrile solution of 2,2,2-

crytand and silver nitrate, and sealed by porous CoralPor tip. The electrode solution consists of 20 mL acetonitrile (anhydrous, Sigma Aldrich) 0.3025 g 2,2,2-crytand (376.49 g/mol., 2.13 mmol., 0.1 M, Sigma), and 0.0336 g silver nitrate (169.88 g/mol., 0.198 mmol., 0.01 M, BASi). This solution also serves as the electrode storage solution. The electrode and solution were kept in a sealed glass jar wrapped in aluminum foil to prevent unwanted exposure to light. This reference is typically found at +0.5V versus Fc^{+}/Fc and allows for accurate measurement of reference potentials without leakage or short-term potential drift. [19]

Electrode Treatment

Each electrode used underwent a pre-polish sonication in acetone, water, and then isopropyl alcohol for approximately 30-60 seconds each to remove any residues left from previous experimentation. Each electrode then underwent a polish with fine alumina slurries of 1.0 μm, 0.3 μm, and 0.05 μm. For each size of alumina slurry all electrodes underwent three hundred figure-eight pattern strokes and then were rinsed before undergoing sonication in type-II deionized water for approximately 90 seconds to remove residual alumina. The electrodes are then sonicated for 90 seconds in isopropyl alcohol to assist in the removal of water. Finally, each electrode was left to dry atop an oven for approximately 25-30 minutes before experimental use.

Electrochemistry Buffers

All buffer systems consist of equal concentrations of acid or base and its conjugate salt. Buffer, pKa value [18] [20] [22], acid component, and base component are as follows:

2,6-dichloroanilinium: pKa 5.0, tetrabutylammonium 2,6-dichloroanilium (synthesized), 2,6-dichloroaniline.

4-cyanoanilinium: pKa 7.0, tetrabutylammonium 4-cyanoanilinium (synthesized), 4-aminiobenzonitrile.

Tosic acid: pKa 8.6, p-toluenesulfonic acid monohydrate (≥98.5%, Sigma-Aldrich), tetraethylammonium p-toluenesulfonate (97%, Aldrich).

Trichloroacetic: pKa 10.7, trichloroacetic acid, trichloroacetate hexafluorophosphate (synthesized).

Dichloroacetic: pKa 15.1, dichloroacetic acid, dichloroacetate hexafluorophosphate (synthesized).

V. NMR Instrumentation

All NMR analysis was performed using a 400 Mhz Bruker NMR and processed with the aid of Bruker Topspin computer software.

VI. Results and Discussion

It has been shown that the dioxovanadium species undergoes a two electron reduction during the catalytic deoxydehydration of glycols. [1] There are two questions at hand concerning this fact. First, will the same $2e^-$ transfer occur if induced electrochemically in the presence of a proton donor/acceptor species? Second, does that reduction and oxidation involve a step-wise or

concerted proton electron transfer? These two questions are assessed through voltammetry, Kouteck-Levich, Tafel, and DPV analysis.

Cyclic Voltammetry

The electrochemical characterization begins with the evaluation of several **CV** backgrounds to review the activity of the individual species being used: the **$TBAPF_6$** electrolyte, the **TBADVP** catalyst, and the 2,6-pyridinedicarboxylic acid (dipic ligand) used to synthesize the vanadium species. The results of all three experiments can be seen in Figure 4a below. It can be clearly seen that the **$TBAPF_6$** electrolyte is inert. The dipic ligand on the other hand shows two clear reduction waves; one at -1.66 V and another at -1.9 V. These events are assumed to be an irreversible two electron transfer to the pyridine ring, the first being a short-lived radical. After the potential switches, an oxidation wave appears at -1.975 V and is assumed to be the removal of the electron that was added at the -1.9 V. The vanadium species shows similar activity at cathodic potentials with a few exceptions. First, the reduction of the pyridine ring occurs at the same onset potential and shows two oxidation waves. Second, hydrogen evolution reaction (**HER**) appears at -2.35 V. Finally, reversible one electron transfers to the vanadium center are present at -1.4 V and at +0.38 V which are in close agreement with literature values. [24] The reduction wave at -0.97 V is unknown but assumed to be associated with the oxo- groups attached to the vanadium center as typical oxygen reduction occurs at approximately the same onset potential in acetonitrile. [6] The oxidation waves present from -0.6 V to +0.1 V are assumed to be associated with the dipic ligand as they are seen in both complex and ligand CVs. The oxidation wave at +0.87 V is also unknown but is assumed to be associated with the metal since it is absent in the dipic **CV**.

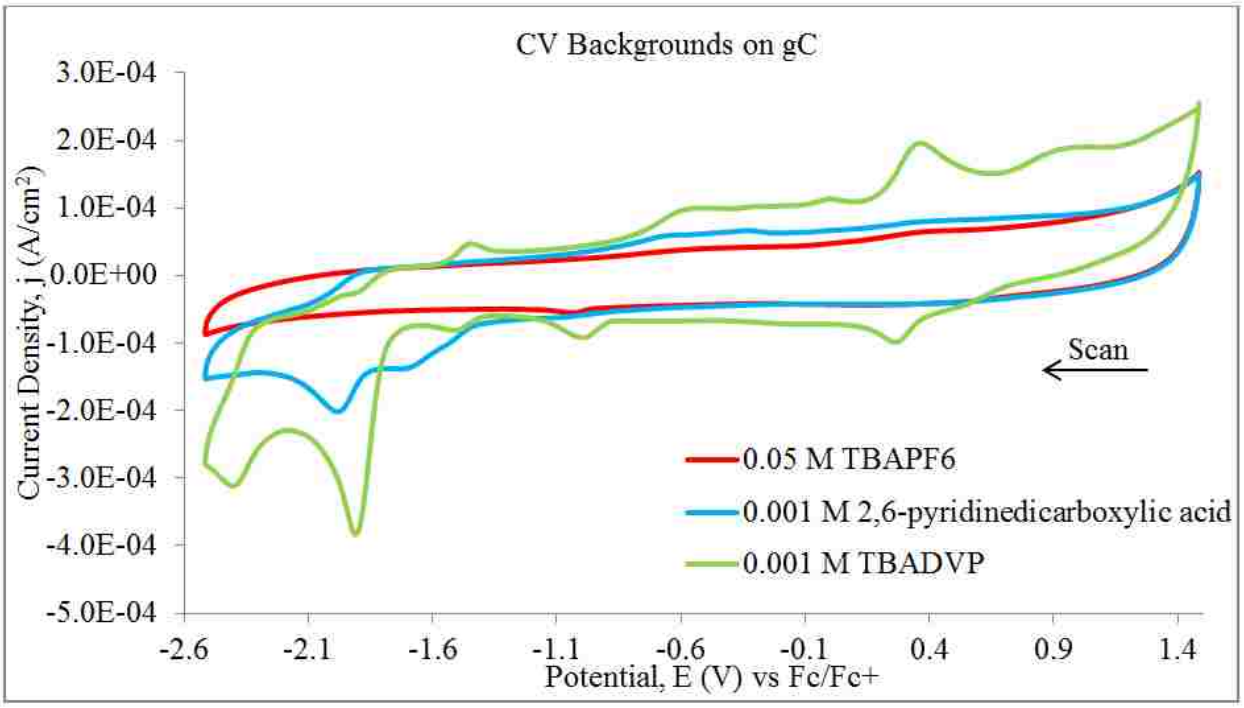

Figure 4a: Background **CV**s of vanadium catalyst, electrolyte, and dipic ligand in acetonitrile on a glassy carbon electrode at a scan rate of 0.1 V/sec.

The next step was to introduce the vanadium catalyst to a proton source. Tosic acid was arbitrarily chosen since it is a good proton source and buffered easily with its conjugate tetraethylammonium salt. Using a complex:buffer ratio of 1:3 led to the best experimental responses. The resulting CV with species backgrounds overlaid can be seen below in Figure 4b.

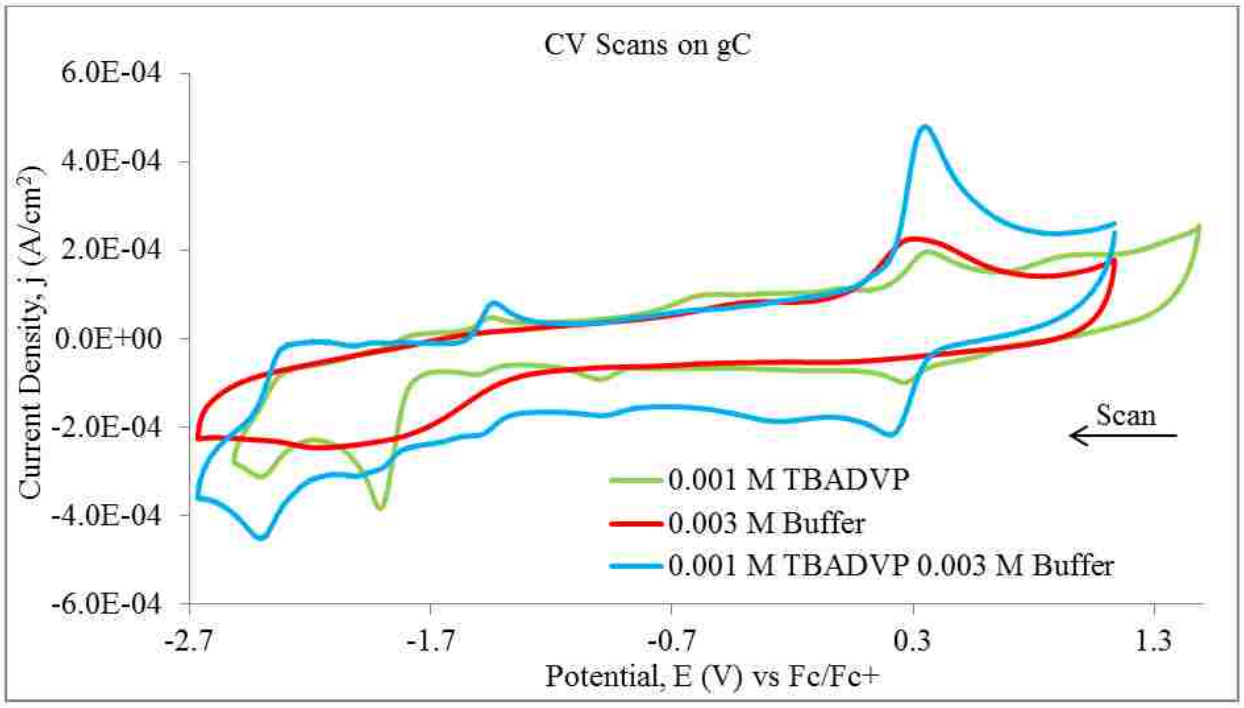

Figure 4b: **CV**s of vanadium complex (blue) in the presence of tosic acid buffer with corresponding backgrounds (green and maroon) on a glassy carbon electrodeat scan rates of 0.1 V/s. All **CV**s performed in an acetonitrile solution containing 0.05 M **$TBAPF_6$**.

The reversible one electron transfers to the vanadium center remain present at -1.4 V and at +0.38 V but have heavily augmented currents due to the presence of tosic buffer. The oxidation wave at +0.319 V is additive with the oxidation of the tosic buffer system which explains the difference between peak oxidation and reduction currents. The peak current for the two electron reduction of pyridine at -1.88 V is not as prevalent due to an overlap with the reduction of tosic acid. Under these conditions the reduction appears to have visibly separated into two redox waves. The HER redox couple has larger currents as expected due to the presence of free protons in solution. It must be noted that upon introduction to free protons a color change from clear to transparent yellow was observed. This is an indication that the vanadium species is protonated; similar to what has been seen in literature. [25]

To evaluate the effect of proton concentration on the redox couple at 0.38 V the buffer ratios were varied to apply an effective pH change. An electrochemical cell containing 35 mL acetonitrile, 0.05 M $TBAPF_6$, 0.001 M TBADVP, and 0.003 M tosic acid buffer was assembled for the analysis. CV sets were performed with Au, Pt, and gC post working electrodes at scan rates of 0.1, 1.0, and 10.0 volts per second. A potential window of 0.4 to 1.15 V, sample interval of 0.001 volts, and a sensitivity of 1.0 E -05 A/V were utilized. At a buffered pH of 8.6 a reversible couple appears at approximately 0.3 V (Figure 5a). A plot of peak current density for the redox couple versus the root of the scan rate (Figure 5b) results in a linear relationship; indicating that the redox is diffusion based and not a surface event.

Between each set of experiments the buffer pH was varied by 0.2 pH units through a pH range of 6.8 to 10.0 with respect to the tosic acid pKa of 8.6 in acetonitrile [18]. This variation in pH was used to construct a short window pourbaix diagram to evaluate the number of electrons transferred in an electrochemical manner through the redox event in question. Below are the CVs and corresponding pourbaix diagrams for all three electrode substrates (Figure sets 6, 7, and 8). When the linear portion of each pourbaix diagram (pH 7.5 to pH 9.0) is taken a slope of approximately 44 mV per decade is observed (Figure 9). This value corresponds to a 3 proton, 4 electron transfer to the vanadium species.

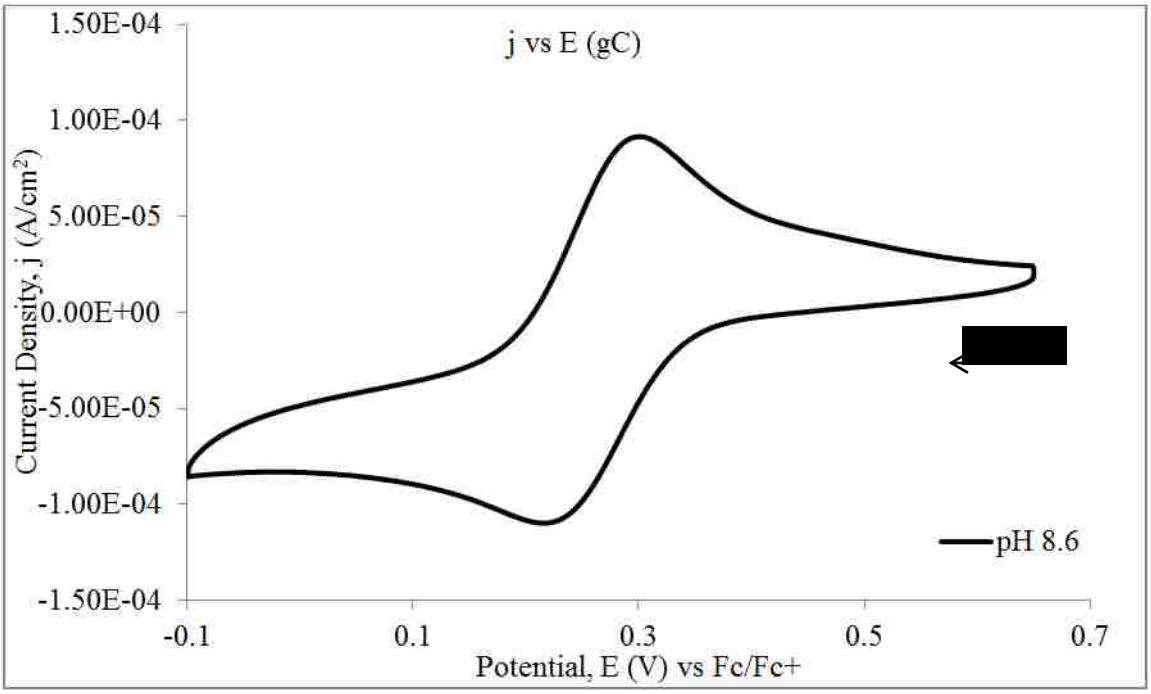

Figure 5a: **CV** of 0.001 M TBADVP, 0.003 M Tosic acid buffer (pH 8.6), 0.05 M **$TBAPF_6$**, in acetonitrile on a glassy carbon post electrode scanned at 0.1 V/sec.

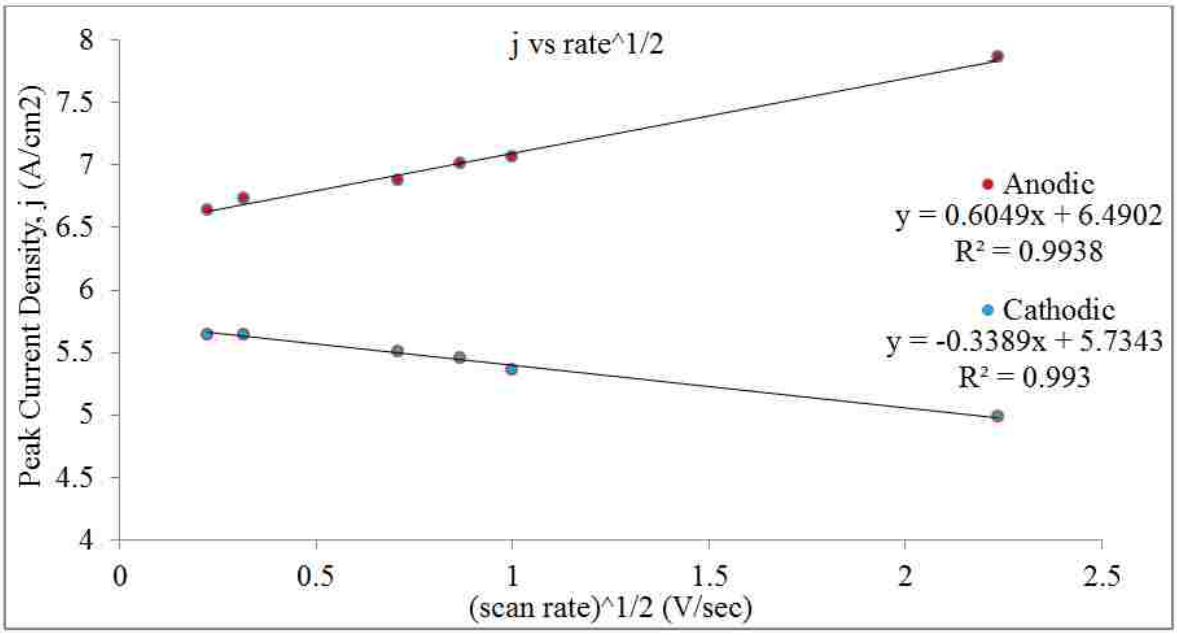

Figure 5b: Plot of peak current density versus the square root of scan rate.

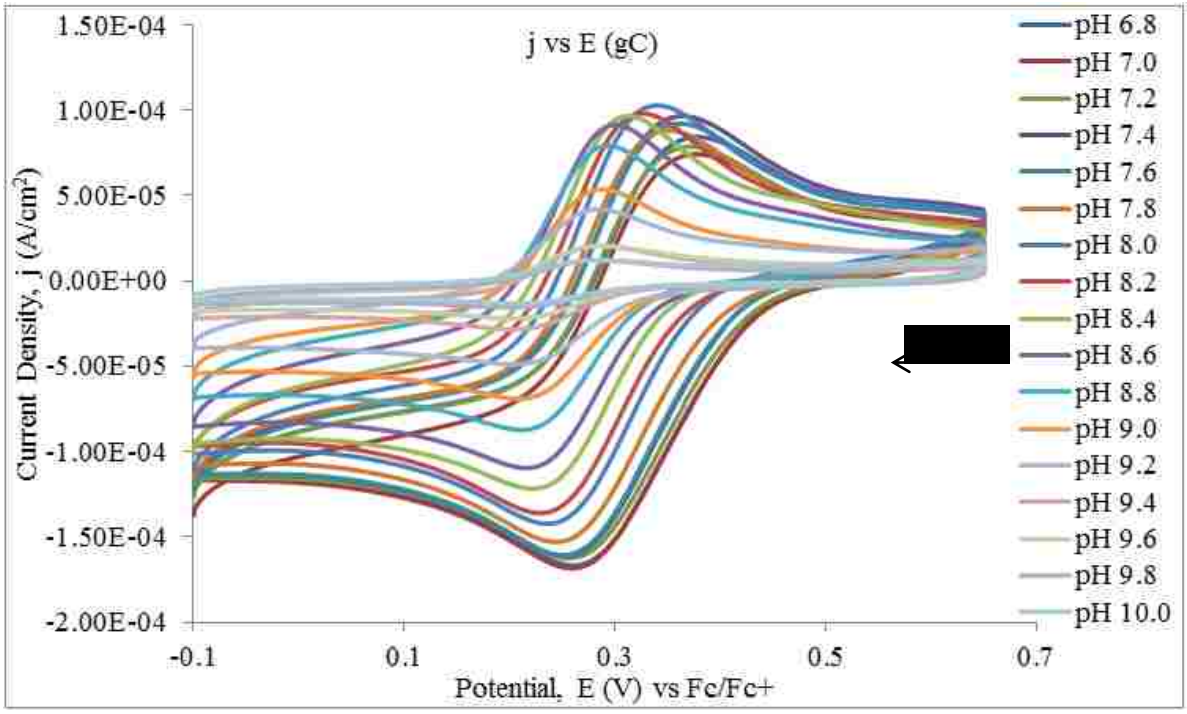

Figure 6a: **CV** set for the effect of pH on potential on a glassy carbon post electrode.

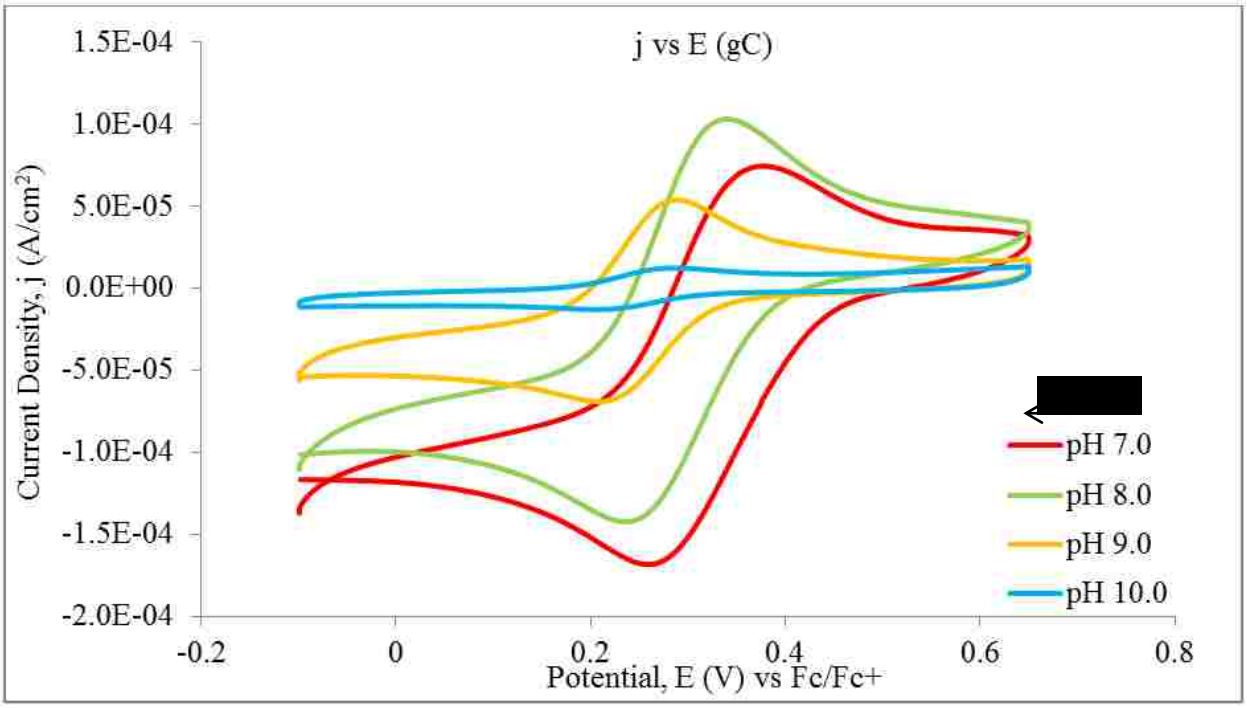

Figure 6b: Truncated **CV** set for the effect of pH on potential on a glassy carbon post electrode.

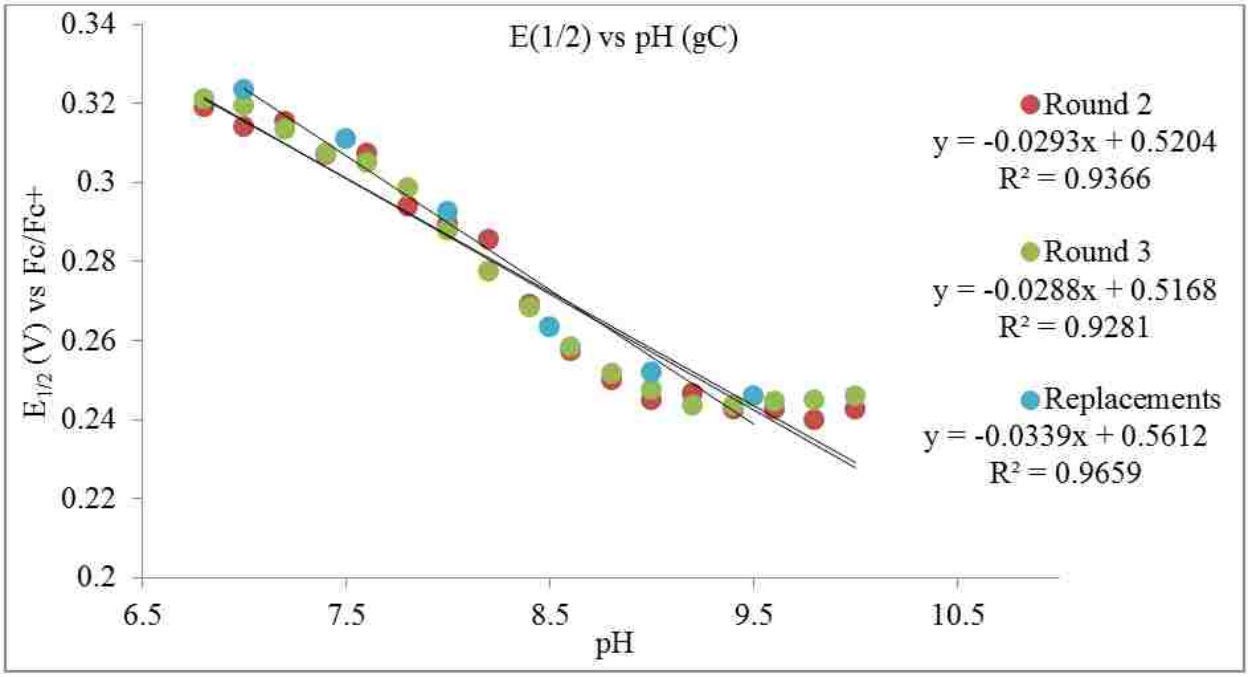

Figure 6c: Pourbaix diagram for effect of pH on potential on a glassy carbon post electrode.

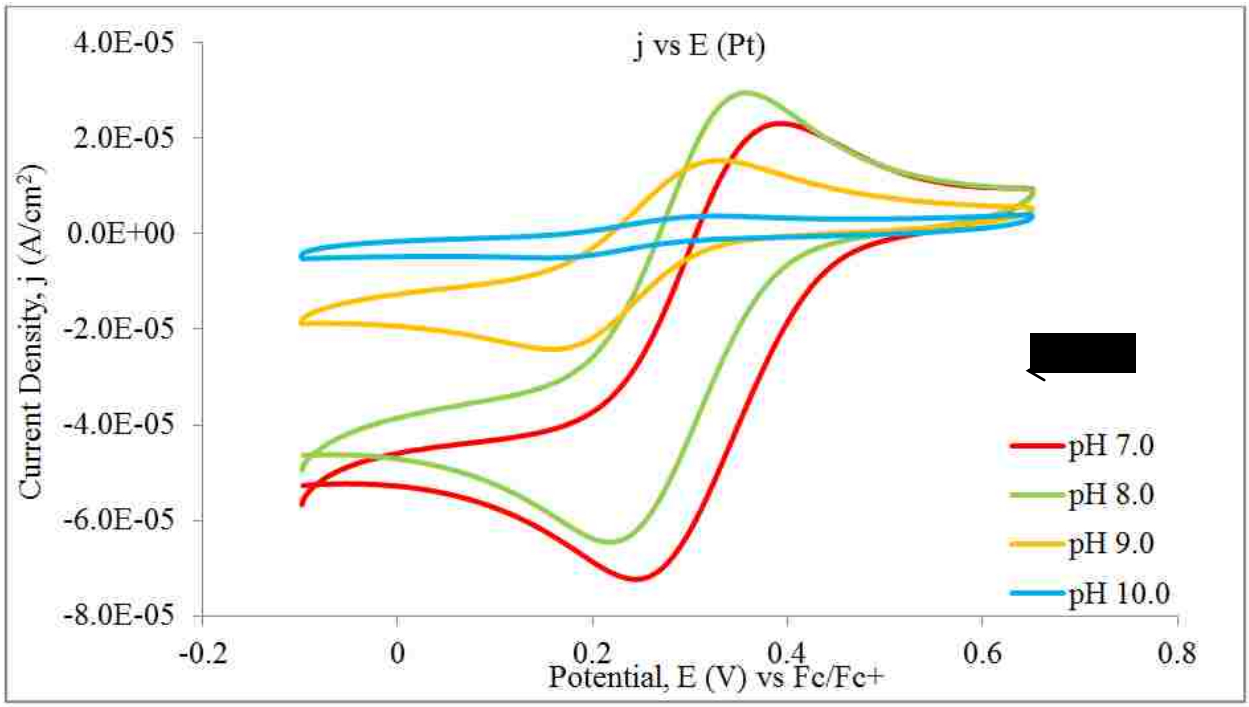

Figure 7a: Truncated **CV** set for the effect of pH on potential on a platinum post electrode.

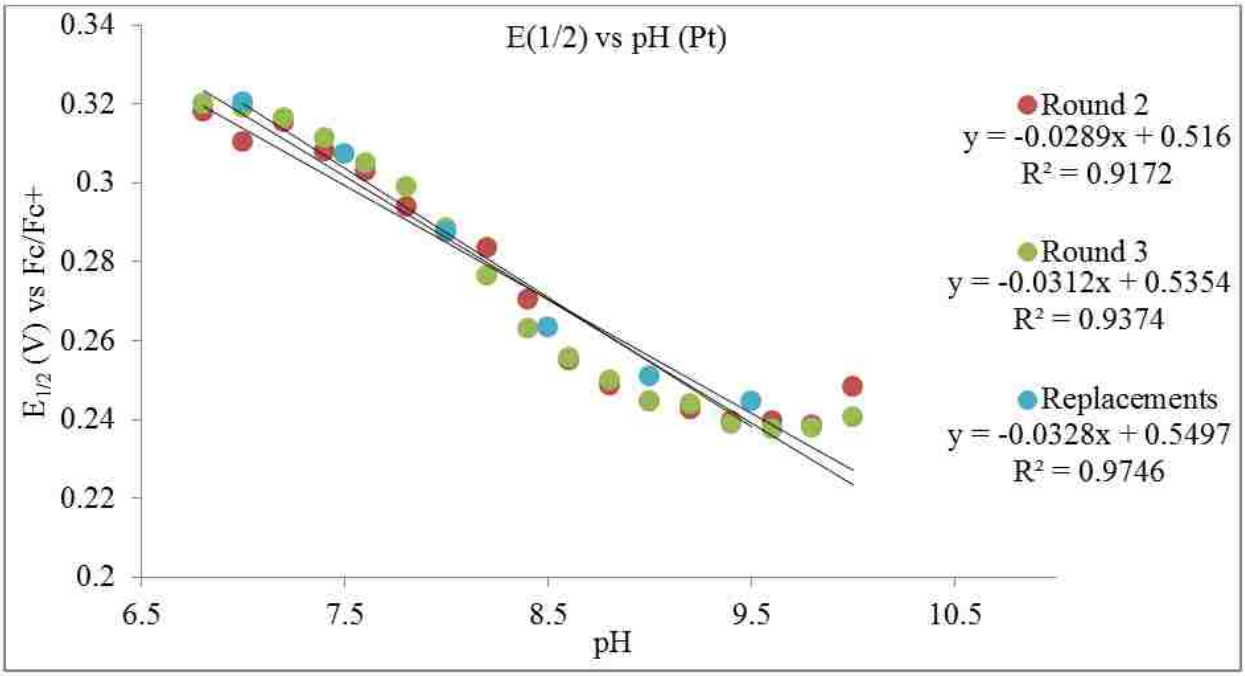

Figure 7b: Pourbaix diagram for the effect of pH on potential on a platinum post electrode

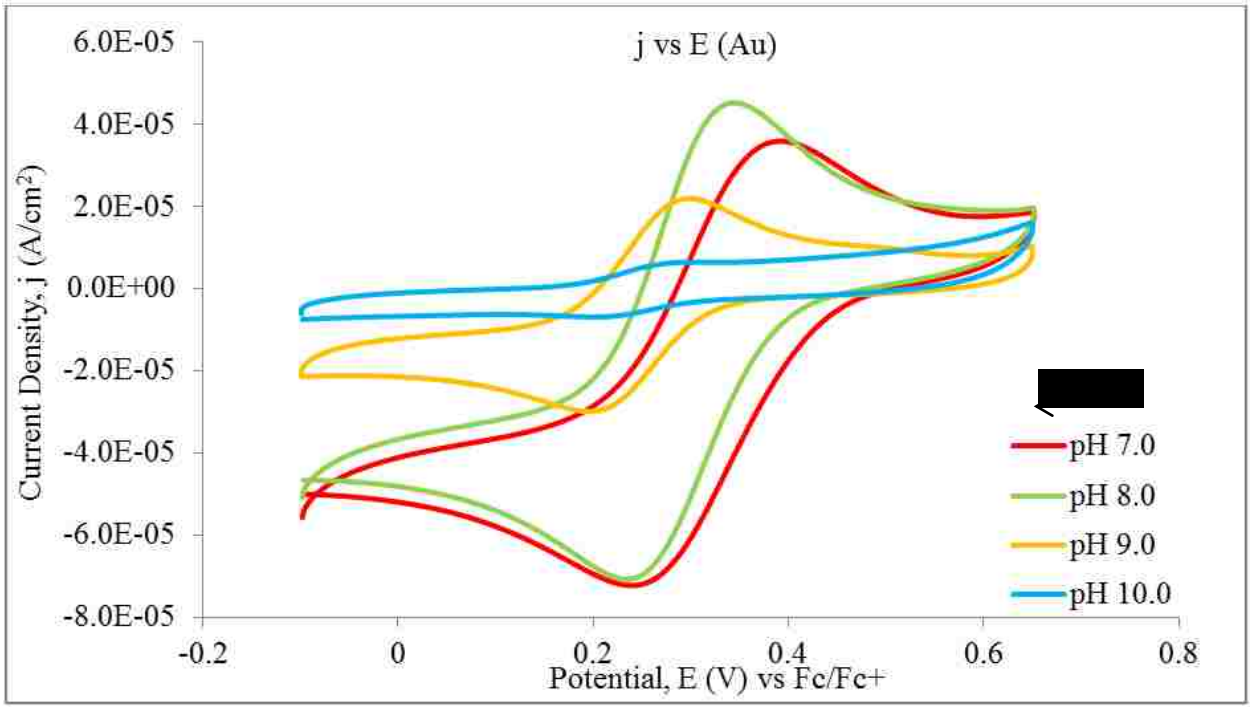

Figure 8a: Truncated **CV** set for the effect of pH on potential on a gold post electrode.

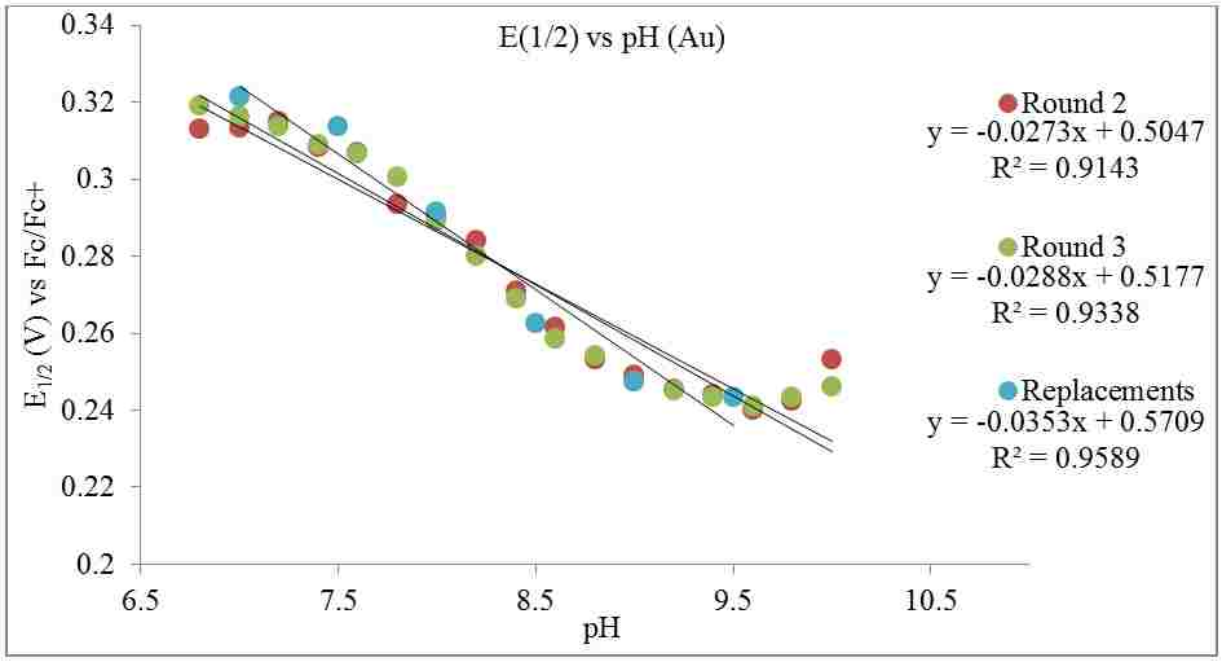

Figure 8b: Pourbaix diagram for the effect of pH on potential on a gold post electrode.

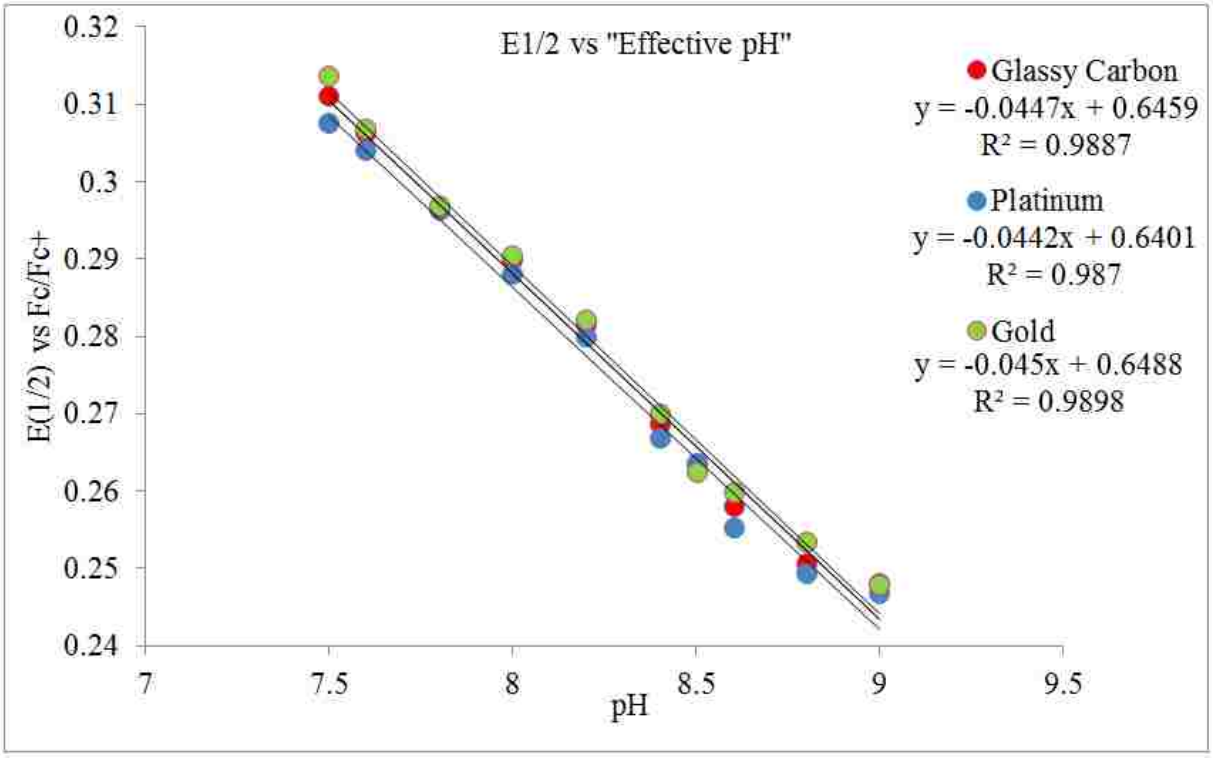

Figure 9: Averaged $E_{1/2}$ values versus pH for each electrode substrate.

To further observe the behavior of the vanadium species the proton environment (subsequently the pH of the electrochemical experiments) must be changed further. This was achieved by selecting buffer systems with pKa values both above and below that of the tosic acid system (pKa 8.6). A literature search turned up numerous possibilities but in the end single protic acid/base systems were chosen based upon their availability and ease of synthesis. [18a-18f] Once decided upon, the chosen systems were initially probed by checking the electrochemical activity of each acid/base species in the absence of its conjugate salt. Figure 10 shows an overlay of **CV**s for species possessing pKa values between 10 and 20 in the absence of buffer using a glassy carbon post electrode. From this data it was determined that only a pKa of 10.7 (trichloroacetic acid) showed an appreciable redox response in the absence of buffer and was set as the upper-limit of the pKa studies.

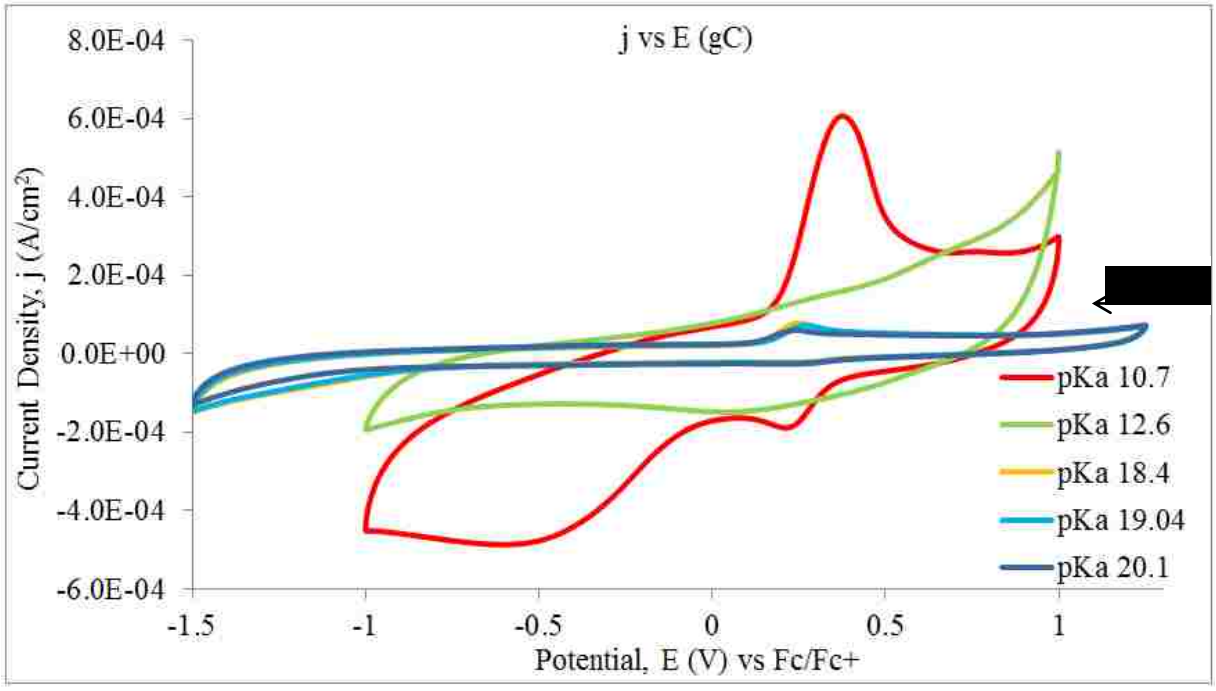

Figure 10: **CV**s for chosen acids in acetonitrile on a glassy carbon post electrode at scan rates of 0.1 V/sec. Conditions: 0.05 M **TBAPF$_6$**, 0.001 M **TBADVP**, and 0.003 M acid species.

The lower limit for pKa was dependent on the ability to synthesize conjugate acid salts and the short list of suitable buffers available to use. After assessing these limitations, conjugate salts were chosen and then synthesis attempted. Only two were successful 2,6-dichloroanilinium and 4-cyanoanilinium. Going forward electrochemistry was performed using a stationary quick change glassy carbon **RDE** out of convenience. Figure 11 is the comparison of the four selected buffer systems. The known, reversible one electron reduction at -1.5 V of the vanadium center stays constant. [24] The catalytic current for this redox event appears to increase as the buffer system is shifted toward neutral conditions and then decrease as the system goes into a more acidic regime (5.0 pH) although it maintains its reversibility.

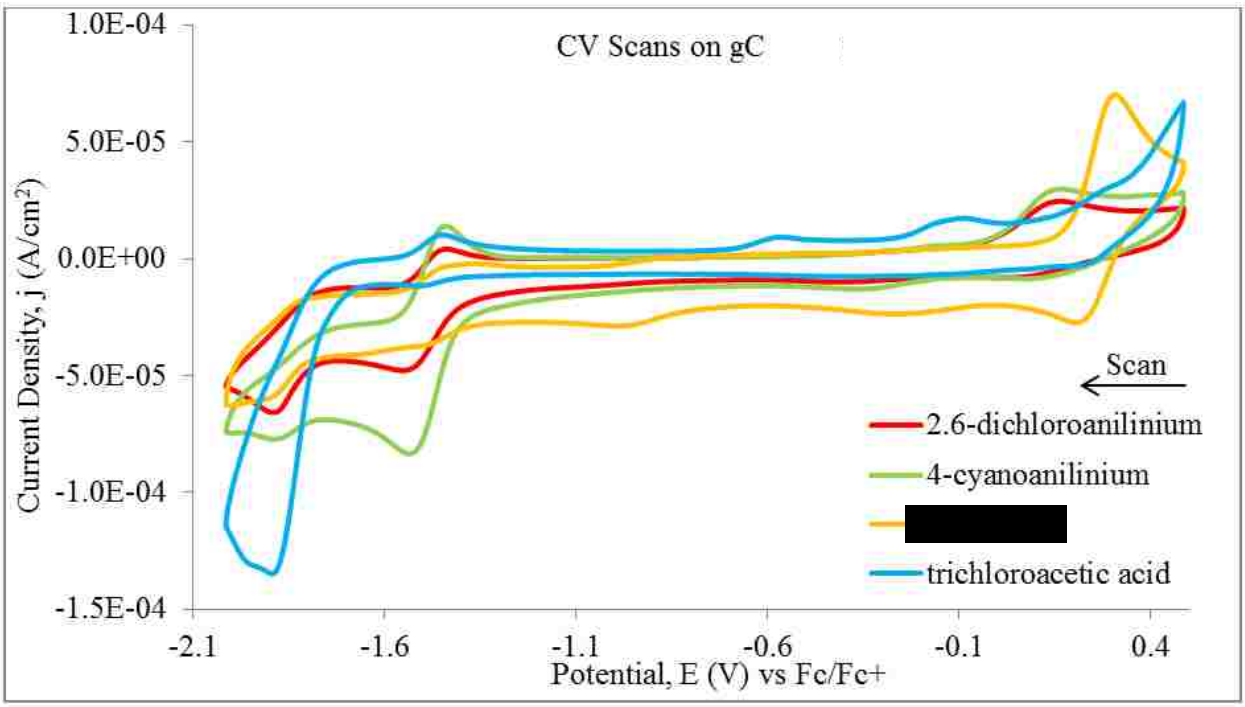

Figure 11: Full window **CV** comparison for chosen buffer systems on a glassy carbon electrode at 0.1 V/s. 0.001 M **TBADVP**, 0.003 M Total Buffer, 0.05 M **$TBAPF_6$**.

The redox couple seen at +0.38 V appears to become irreversible and unexpectedly more cathodic as the buffer system becomes more acidic. A closer look at the 4-cyanoanilinium/4-

aminobenzonitrile buffer system turned up something fascinating. At faster scan rates (Figure 12a) the **CV**s show two oxidation waves. When the electrolyte and buffer background is subtracted the events become a little clearer (Figure 12b). The first wave at 0.13 V appears to be coupled to the reduction wave seen at 0.046 V implying reversible electron transfer. The second oxidation wave at 0.379 V shows a large diffusion event that lacks a well-defined reduction on return scan.

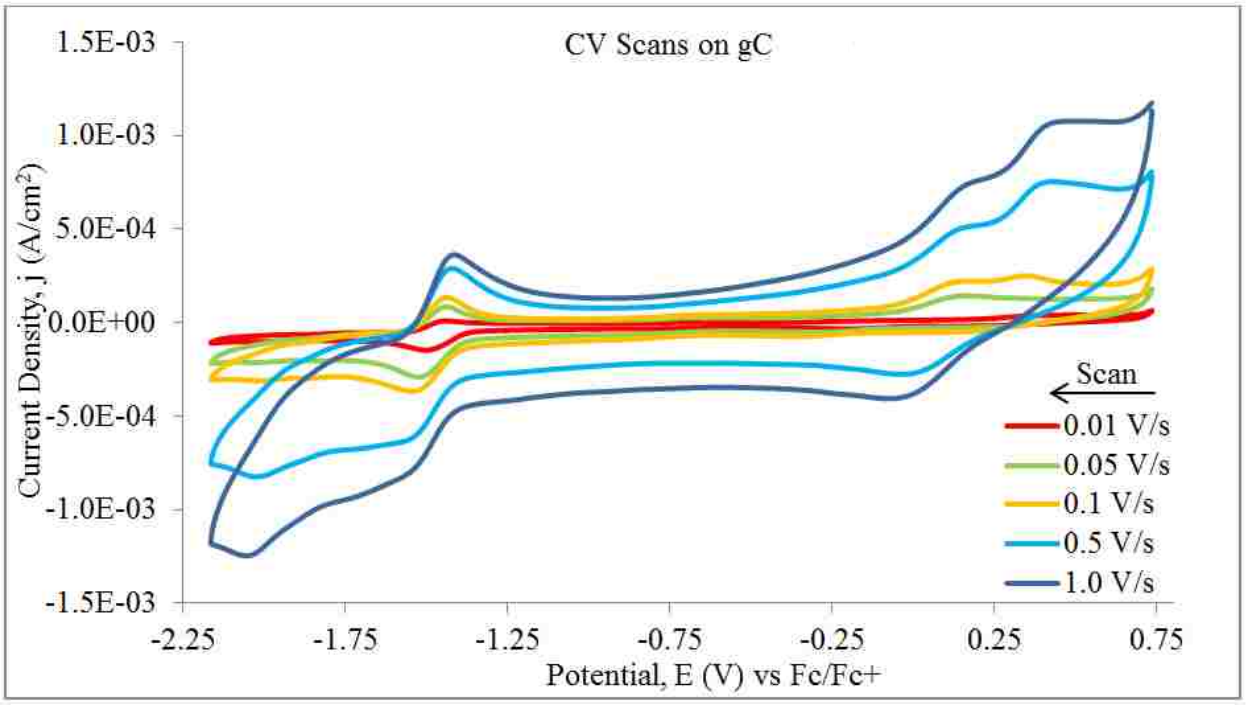

Figure 12a: 4-cyanoanilinium/4-aminobenzonitrile system at different scan rates. 0.05 M **$TBAPF_6$**, 0.001 M **TBADVP**, 0.003 M Buffer, in acetonitrile on a glassy carbon electrode.

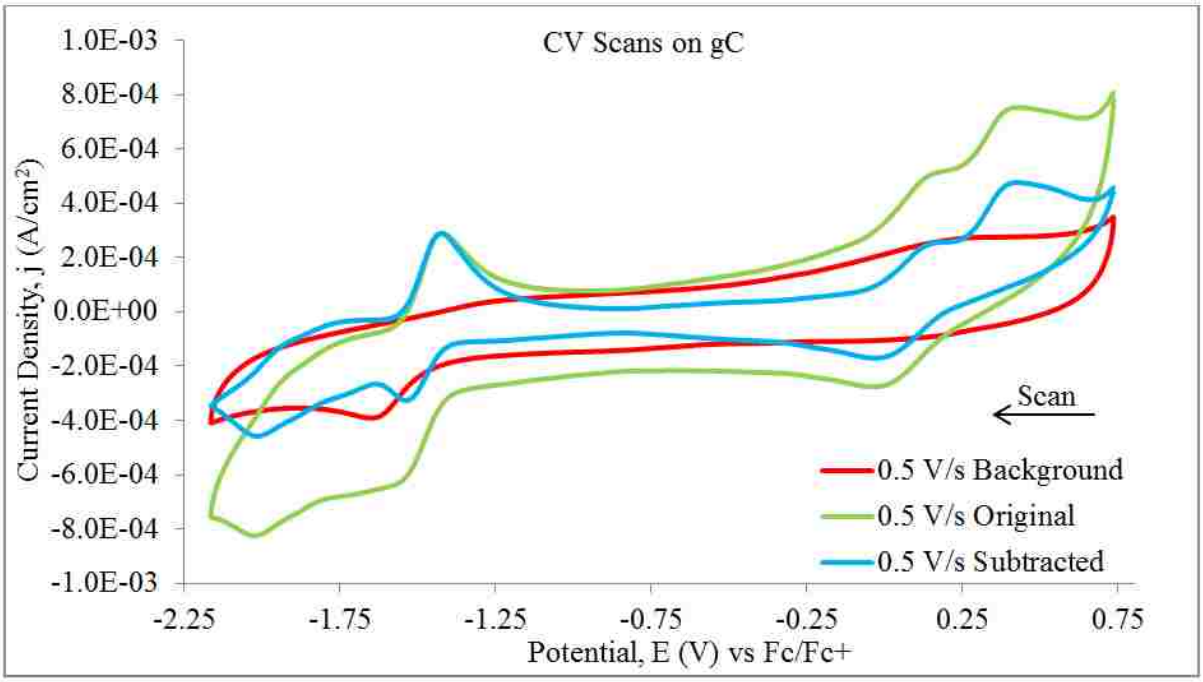

Figure 12b: Buffer and electrolyte background (red), 4-cyanoanilinium system as observed (green), system with background subtracted (blue).

Differential Pulse Voltammetry

To get a better idea of the reversibility of electron transfer to the vanadium complex, **DPV** techniques were implemented for each buffer system. This enables to detection of electron transfers that may not have been detected (observed) using cyclic voltammetry. Parameters used to obtain all DPVs are as follows: Initial E -2.0 V to -1.65 V, Final E 1.25 V to 2.0 V, Increment E 0.002 V, Pulse Amplitude 0.050 V, Pulse Width 0.5 seconds, Sample Width 0.167 seconds, Pulse Period 1 second, Quiet Time 2 seconds, and Sensitivity of 0.001 A/V. The first buffer system to be approached in this manner was the tosic acid system. Background **DPV**s were obtained for the electrolyte, electrolyte with buffer, and electrolyte with vanadium species (Figure 13a). DPVs of the entire electrochemical system were then obtained in triplicate at a pH of 8.6 (Figure 13b). 0.05 M **$TBAPF_6$**, 0.003 M tosic buffer, and 0.001 M **TBADVP**. The experiment was performed in acetonitrile on a glassy carbon **RDE**.

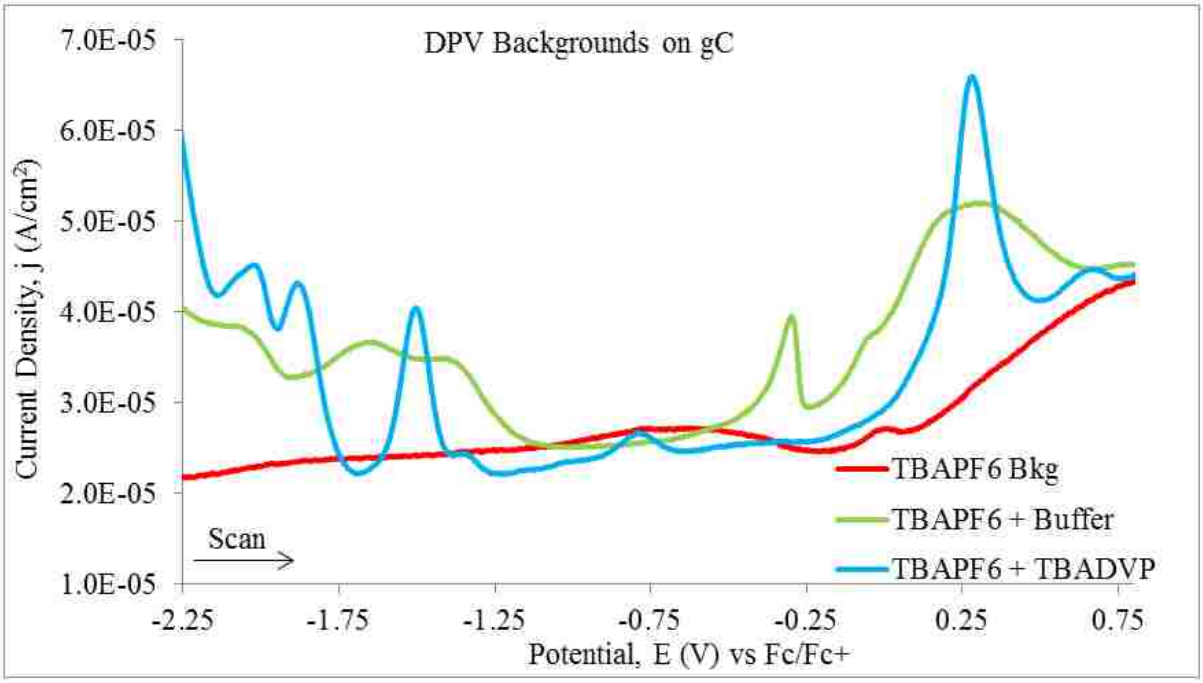

Figure 13a: Background **DPV**s for each component of the pH 8.6 tosic buffer experiment.

While background **DPV**s show activity for each component of the experiment they are all at very low current densities (5 e-05 A/cm^2) which is near the baseline for an "all in" experimental **DPV**. Despite this fact the activity for the **TBADVP** is clearly seen: two reversible electron transfers associated with the pyridine ligand (-2.0 V and -1.9 V), a reversible one electron transfer to the metal ligand at -1.5V, and a reversible one electron transfer at 0.25 V. The same characteristic peaks can be seen in the experimental **DPV**s with a couple additional signals due to electrolyte (the shoulder at 0.03 V) and buffer (the peak seen at approximately -0.6 V). The peak potentials are shifted approximately 40 mV cathodically which is a typical occurrence. [6]

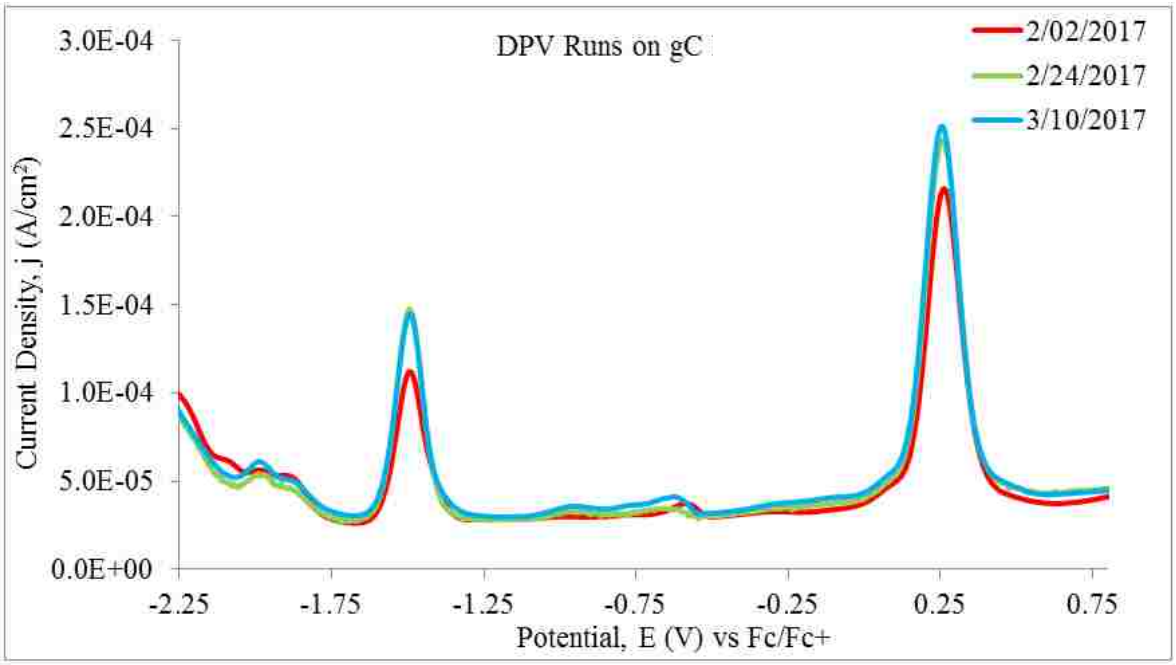

Figure 13b: **DPV**s for the pH 8.6 tosic buffer experiment.

The next route was to change the buffer system to see if any experimental change could be observed; the 4-cyanoanilinium buffer system was chosen first. Experiments were performed in acetonitrile and consisted of 0.05 M **TBAPF$_6$**, 0.001 M **TBADVP**, and 0.003 M buffer. A stationary glassy carbon **RDE** electrode was used for all analysis. A background comparison of each component can be seen in Figure 14a. The 4-cyanoanilinium/4-aminobenzonitrile buffer system is heavily active at potentials over 0.6 V. Two large reversible signals appear in the background but well outside the activity window for **TBADVP**. There is a shoulder band in the buffer activity window from -0.25 V to 0.5 V that only appears if the potential is allowed to surpass 0.6 V. The DPV scans for the entire system (Figure 14b) shows the transfer of multiple electrons to the vanadium species in the potential window of 0.0 V to 0.6 V. The one electron transfer to the vanadium center appears at -1.5 V and the electron transfer to the pyridine ring appears as a broad wave at approximately -1.8 V.

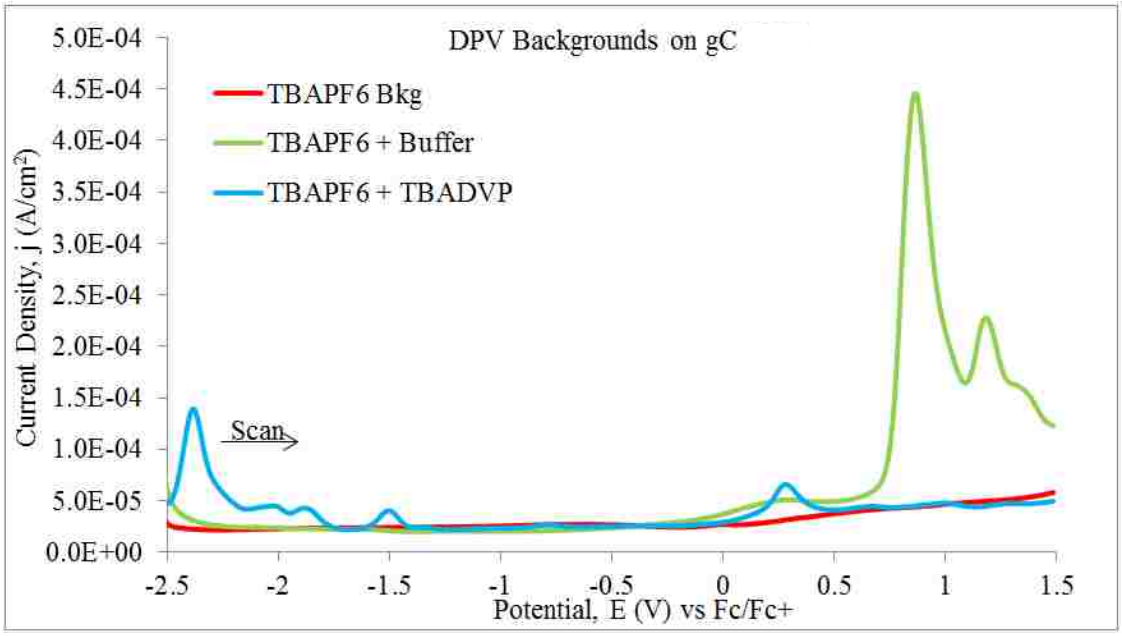

Figure 14a: **DPV** backgrounds of 0.05 M **$TBAPF_6$**, 0.001 M **TBADVP**, and 0.003 M 4-cyano buffer in acetonitrile on a glassy carbon electrode.

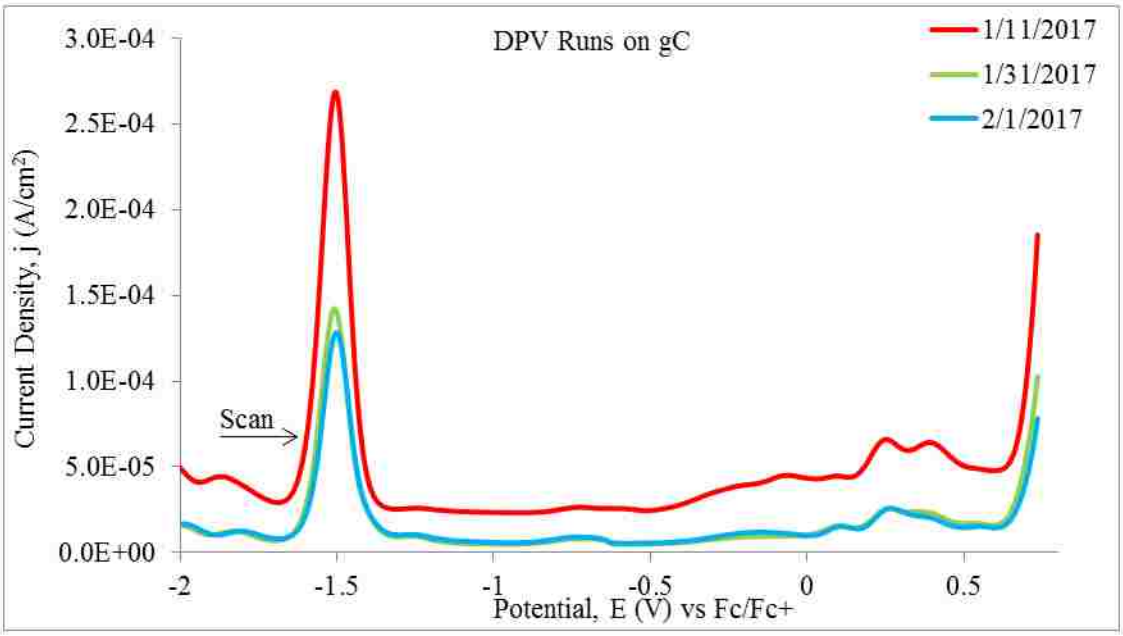

Figure 14b: **DPV**s in triplicate of 0.05 M **$TBAPF_6$**, 0.001 M **TBADVP**, 0.003 M 4-cyano buffer in acetonitrile on a glassy carbon electrode.

The trichloroacetic acid and 2,6-dichloroanilinium buffer systems did not yield substantial **DPV** results. The signals of both buffer systems dwarfed any **TBADVP** activity that could be detected.

Koutecky-Levich Analysis

To assess the number of electrons transferred electrochemically **KL** analysis was implemented during most experiments. **RDE** rotation sets were 250 RPM-2000 RPM by steps of 250 RPM (and occasionally 2250 RPM). To prove working knowledge and equipment technique the determination of the diffusion coefficient for ferrocene was first tackled. For this analysis published techniques were followed. [28][29] The area used for all calculations was the predetermined 0.19635 cm^2. The kinetic viscosity used in all determinations was the same as literature values for the solvent and electrolyte used (2.46 cm^2/sec). [28][30] After several runs the diffusion coefficient was calculated to be 2.23E-05 cm^2/sec, which is well within agreement of literature values. [6] **KL** analysis then moved to that of **TBADVP**. All figures are on glassy carbon unless stated otherwise. All **KL** analysis was performed for each buffer system although the electron transfer behavior does not agree between systems. The primary buffer system used to evaluate electron transfer at 0.25 V was determined to be tosic acid as it is the only system to have exhibited dependence on donor/acceptor ratio. The kinetic viscosity used for calculations is 2.15 cm^2/sec, a value determined through the use of a glass capillary viscometer. A primary example of consistency can be seen in Figure 15a in which **CA** was used to achieve diffusion limiting current in a tosic system of pH 8.6 at 0.4 V. This shows a slope that represents a one electron transfer to the vanadium species with an average molecular diffusion of 3.36E-06 cm^2/sec. The intercepts show an average kinetic current density that equals 1.98 mA/cm^2. A similar comparison and conclusion can be seen in Figure 15b in which a **KL** analysis is

performed using **LSV** current densities at the same 0.4 V potential. The slopes achieved represent a one electron transfer to the vanadium species with an average molecular diffusion equaling 3.95E-06 cm^2/sec. The resulting intercepts yield an average kinetic current density of 0.83 mA/cm^2. The **LSV-KL** being half the concentration it is expected that the resulting kinetic currents are half of those seen in the **CA-KL** analysis. The two calculated diffusion coefficient values imply a molecular weight around the vicinity of 481.0 g/mol. [31] Such a weight points to the electrochemical generation of a **TBADVP** dimer through the overall transfer of two electrons.

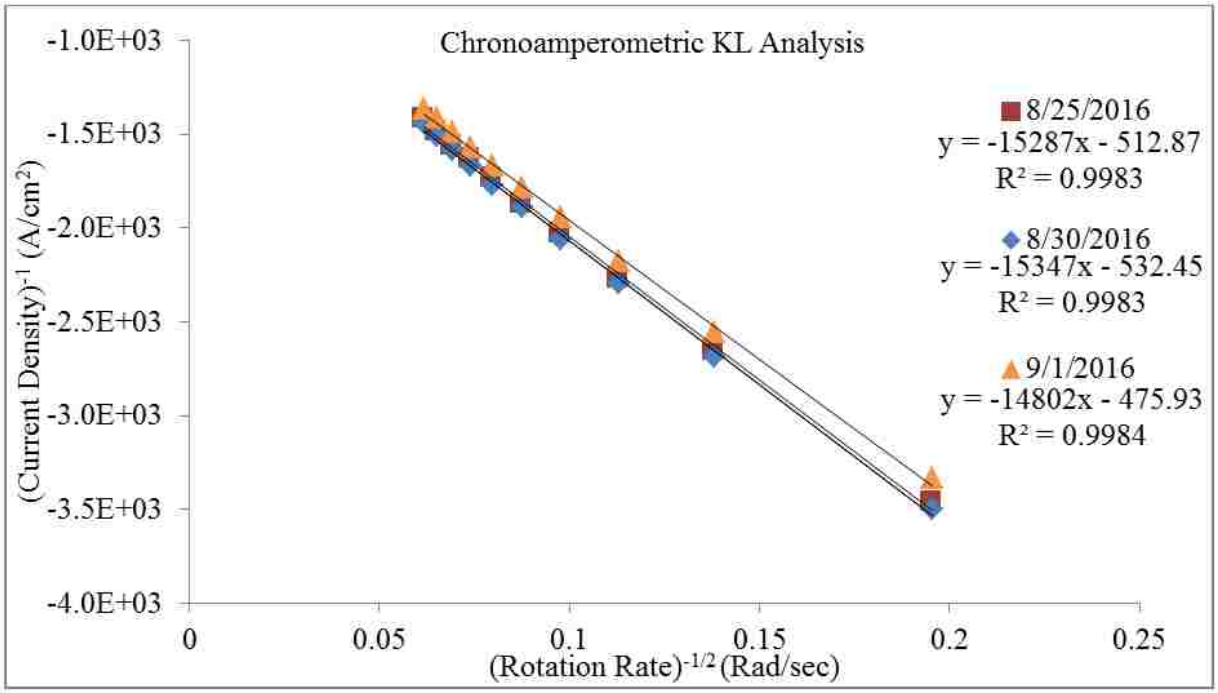

Figure 15a: **CA-KL** of 0.05 M **$TBAPF_6$**, 0.002 M **TBADVP**, and 0.006 M tosic buffer (pH 8.6).

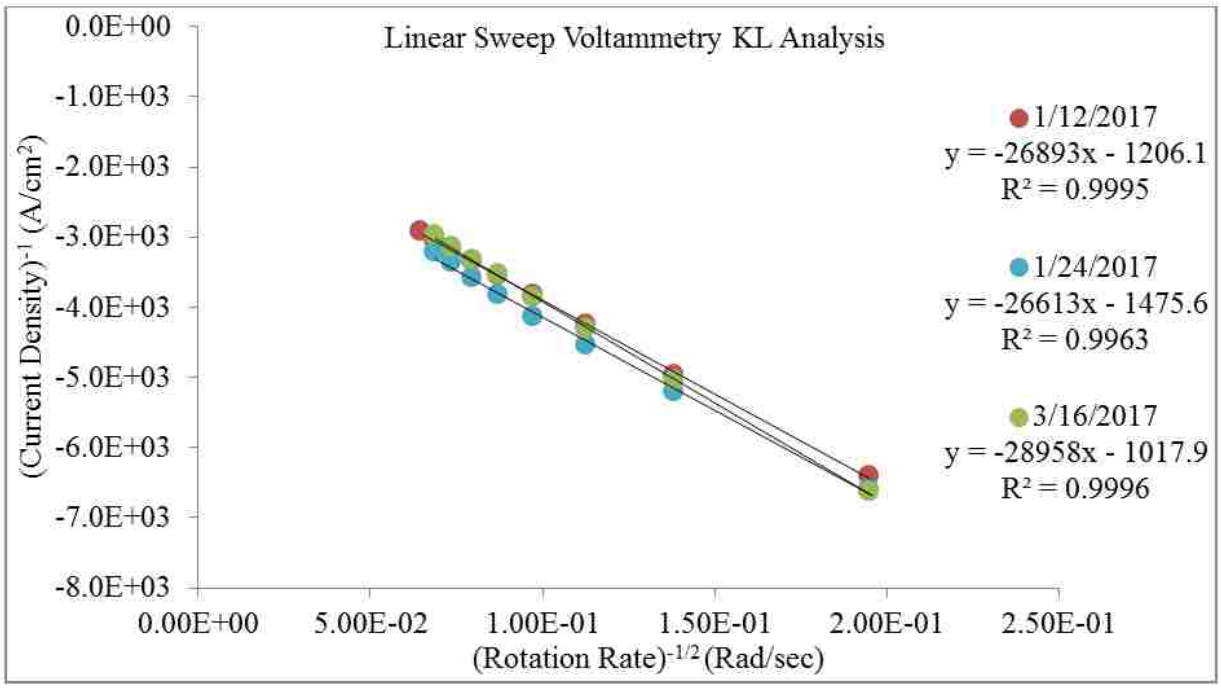

Figure 15a: **LSV-KL** of 0.05 M **$TBAPF_6$**, 0.001 M **TBADVP**, and 0.003 M tosic buffer (pH 8.6).

Tafel Analysis

Tafel analysis was performed on the **TBADVP**/tosic buffer system at pH 8.6. The initial three trials are plots shown in Figure 16a (uncorrected) and 16b (corrected cathodic branches only) are individual diffusion limited current density values taken at 2000 RPM. The potential was stepped +5 mV and held for twenty-five seconds for each current determination. The calculated transfer coefficient (α) values were calculated to be an average of 0.25 (assuming a one electron transfer). This value is representative of a species that favors oxidation. The cathodic branch tafel slopes correspond to a value of approximately 250 mV. The kinetic current density values (j_0) for round 1, 2, 3 are 0.088, 0.067, and 0.083 mA/cm^2 respectively. This gives an average j_0 value of 0.078 mA/cm^2 which results in an electron transfer rate constant (k^0) of 4.03E-04 cm/sec, which is quite slow. These Tafel results hint at a more complicated multi-step electron transfer that is rate-

limited by the initial electron transfer to the vanadium species and a second (possibly faster) transfer in which a dimer is formed.

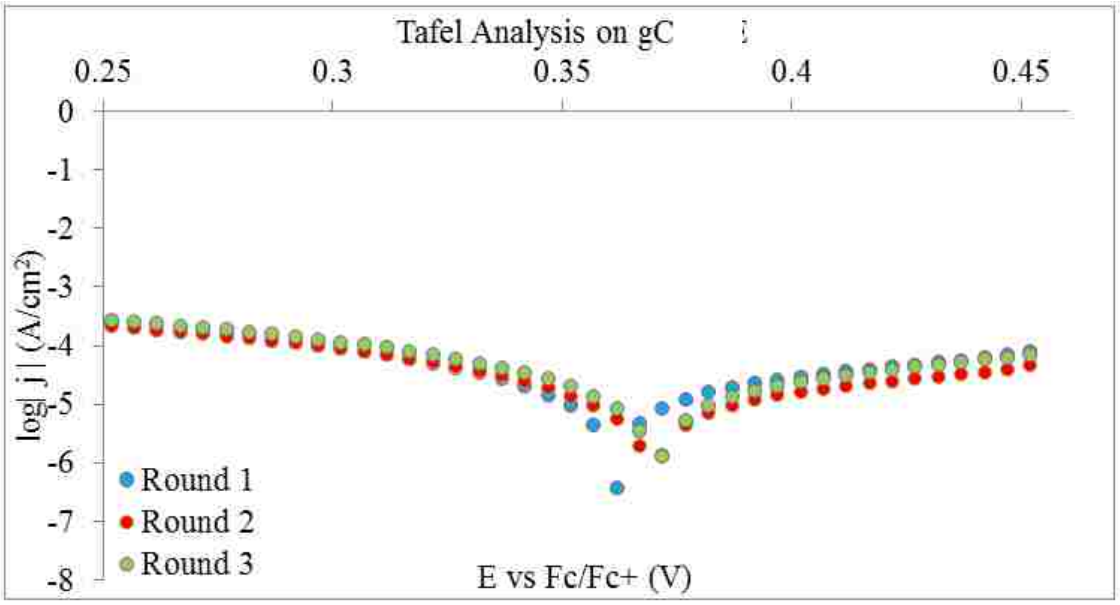

Figure 16a: Tafel Plots (uncorrected to η).

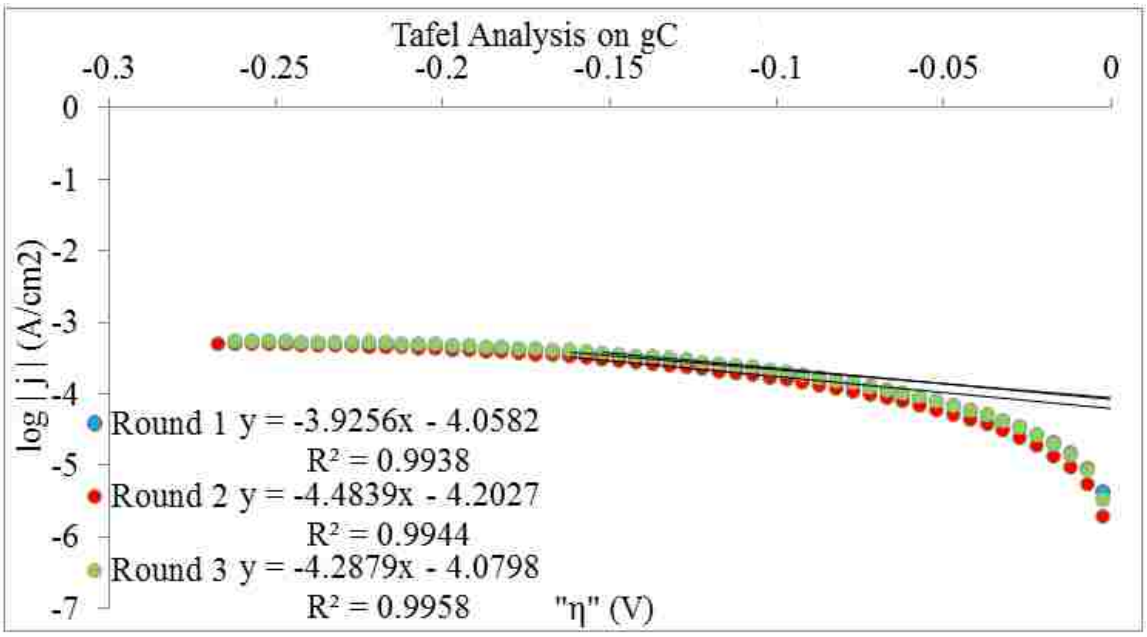

Figure 16b: Tafel plots (Corrected to η) 0.05 M **$TBAPF_6$**, 0.002 M **TBADVP**, 0.006 M tosic buffer (pH 8.6) on a glassy carbon electrode. All points taken at 2k RPM.

ETOF Analysis

To verify diffusion coefficient calculations, the **TBADVP**-tosic buffer system was evaluated using electrochemical time of flight analysis. The experiment was conducted on a platinum electrode array in an acetonitrile solution containing 0.066 M **$TBAPF_6$**, 0.015 M total tosic buffer, and 0.005 M **TBADVP**. The reduced species was generated at 0.4 V and subsequently oxidized at a potential of 0.8 V. An iteration total of n=10 was used resulting in a diffusion coefficient value of 3.9E-06 ±0.2 $vcm^2/sec.$ This value is in close agreement and confirms previously calculated values.

VII. Conclusion

The **TBADVP** species shows robust electrochemical activity. It undergoes multiple reversible electron transfers to the metal center. While the transfer at -1.5 V is clearly a reversible one electron transfer the redox event at +0.25 V is much more complicated and hard to define. **CV** studies indicate that the transfer is reversible, albeit slow, that is diffusion controlled. A change in proton concentration results in a Pourbaix slope that indicates multiple electrons and protons are involved, specifically four electrons and three protons. **DPV** studies, while difficult to quantify, tell a different story: a reversible one electron transfer. **KL** studies, backed up by an **ETOF** verified diffusion coefficient, have the same one electron assessment. The final technique utilized, Tafel analysis, sheds some light on the situation. The cathodic transfer coefficient of 0.25 and Tafel slope of 240+ mV imply one of two things either the species is oxidized easily or the electron transfer is two events. **CV** scans show a single reversible electron transfer at slow scan rates but a second oxidative wave comes out at faster scan rates. This separation of one oxidation into two points (possibly two separate events). It is believed that these two events are a

rate-limited electron transfer followed by the transfer of a second electron and the creation of a dimer that slowly diffuses away from the electrode surface. Both the heterogeneous electron transfer rate constant and diffusion coefficient point to such a species that possesses a molecular weight of approximately 481 g/mol. More evidence to a likely dimer is that the species starts out protonated while in acidic solution, making a good starting point for dimerization to occur. While this mechanism is completely up in the air, a postulated structure with a molecular weight similar to that predicted is shown in Figure 17.

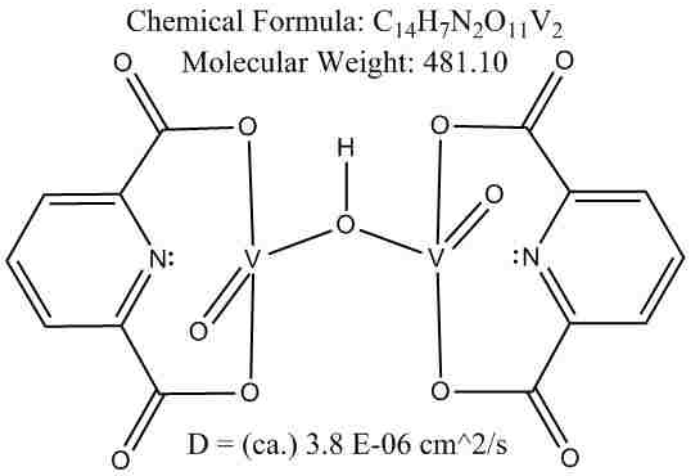

Figure 17: Possible structure for the electrochemically generated **TBADVP** dimer.

While not out the realm of possibility, this structure could be confirmed through chemical reduction and recrystallization. In vitro IR-analysis of the disappearance of metal-oxygen signals would also be an appropriate means of detection. Further study of **TBADVP**, such as bulk electrolysis, will be necessary to assess its ability to catalytically perform **DODH** in the absence of sacrificial reductants.

VIII. References

[1] Chapman, G.; Nicholas, K. M. Vanadium-catalyzed deoxydehydration of glycols. *Chem. Commun.* 2013, 49, 8199-8201.

[2] Gopaladasu, T. V.; Nicholas, K. M. Carbon Monoxide (CO)- and Hydrogen-Driven, Vanadium-Catalyzed Deoxydehydration of Glycols. *ACS Catal.* 2016, 1901-1904.

[3] Saveant, J. Concerted Proton-Electron Transfers: Fundamentals and Recent Developments. *Annual Rev. Anal. Chem.* 2014, 7, 537-560.

[4] Waidmann, C. R.; Zhou, X.; Tsai, E. A.; Kaminsky, W.; Hrovat, D. A.; Borden, W. T.; Mayer, J. M. Slow Hydrogen Atom Transfer Reactions of Oxo- and Hydroxo-Vanadium Compounds: The Importance of Intrinsic Barriers. *J. Am. Chem. Soc.* 2009, 131, 4729-4743.

[5] Warren, J. J.; Tronic, T. A.; Mayer, J. M. Thermochemistry of Proton-Coupled Electron Transfer Reagents and its Implications. *Chem. Rev.* 2010, 110, 6961-7001.

[6] Bard, A. L.; Faulkner, L. R. *Electrochemical Methods: Fundamentals and Applications;* Wiley: New York, 1980.

[7] Revie, R. W.; Uhlig H. H.; Verink, E. D. *Uhlig's Corrosion Handbook;* Wiley: New York, 2000. "Simplified Procedure for Constructing Pourbaix Diagrams."

[8] Day, V. W.; Klemperer, W. G.; Yagasakl, A. Synthesis and Structure of the New Organometallic Polyoxovanadates, $\{[(Bu_4\text{-}C_8H_{12})Ir]_2(V_4O_{12})\}^-$ and $[(Bu_4\text{-}C_8H_{12})Ir(V_4O_{12})]^-$. *Chem. Lett.* 1990, 19, 1267-1270.

[9] Zhao, D.; Ordered Mesoporous Graphitized Pyrolytic Carbon Materials: Synthesis, Graphitization, and Electrochemical Properties. *Journal of Materials Chemistry.* 2012, 22, 8835-8845. Supplementary Information

[10] Cook, G. K.; Andrews, M. A. Toward Nonoxidative Routes to Oxygenated Organics: Stereospecific Deoxydehydration of Diols and Polyols to Alkenes and Allylic Alcohols Catalyzed by the Metal Oxo Complex (C5Me5)ReO3. *J. Am. Chem. Soc.* 1996, 118, 9448-9449.

[12] Izutsu, K.; *Electrochemistry in Nonaqueous Solutions*; Wiley, New York, 2002.

[15] *Petroleum Supply Annual.* U.S. Energy Information Administration, September 2016.

[16] Peters, J.; Mutnean, M.; Janssens_Maenhout, G.; *Trends in global CO2 emissions: 2016 Report;* Netherlands Environmental Assessment Agency, The Hague, 2016. Accessed online on 3/20/2017: "http://edgar.jrc.ec.europa.eu/news_docs/jrc-2016-trends-in-global-co2-emissions-2016-report-103425.pdf"

[17] Gandini, A.; Basile, S.; Albonetti, F.; Cavani; *Chemicals and Fuels from Bio-Based Building Blocks.* John Wiley & Sons, Inc., New York, 2016.

[18a] Dempsey, J.L.; Ullman, A.C.; Rountree, E.S.; Martin, D.J.; McCarthy, B.D.; Electrochemical reduction of Brønsted acids by glassy carbon in acetonitrile-implications for electrocatalytic hydrogen evolution. *Inorg. Chem*. 2014, 53, 8350−8361.

[18b] Leito, I.; Willner, H.; Bernhardt, E.; Yagupolskii, L.M.; Yagupolskii, Y.L.; Garlyauskayte, R.Y.; Koppel, I.; Kaljurand, I.; Mäemets, V.; Raamat, E.; Saame, J.; Rodima, T.; Kütt, A.; Equilibrium Acidities of Superacids. *J. Org. Chem*. 2011, 76, 391-395.

[18c] Leito, I.; Koppel, I.; Mäemets, V.; Rodima, T.; Sooväli, L.; Kütt, A.; Kaljurand, I.; Extension of the Self-Consistent Spectrophotometric Basicity Scale in Acetonitrile to a Full Span of 28 pKa Units: Unification of Different Basicity Scales. *J. Org. Chem. 2005*, 70, 1019-1028.

[18d] Diedenhofen. M.; Klamt, A.; Kütt, A.; Kaljurand, I.; Leito, I.; Eckert, F.; Prediction of Acidity in Acetonirile Solution with COSMO-RS. *Wiley Interscience*. 2008, 799-810.

[18e] Koppel, I.; Yagupolskii, L.M.; Vlasov, V.M.; Sooväli, L.; Kaljurand, I.; Leito, I.; Kütt, A. A Comprehensive Self-Consistent Spectrophotometric Acidity Scale of Neurtral Bronsted Acids in Acetonitrile. *J. Org. Chem*. 2006, 71, 2829-2838.

[18f] Izutsu, K.; Acid-Base Dissociation Constants in Dipolar Aprotic Solvents. *International Union of Pure and Applied Chemistry Chemical Data Series No. 35*. Blackwell Scientific Publications, England, 1990.

[19] Lewandowski, A.; Osinska, M.; Swiderska-Mocek, A.; Galinkski, M.; A Cryptate Reference Electrode for Ionic Liquids. *Electroanalysis*. 2008, 20, 1903-1908.

[20] Robers, J.A.S.; Bullock, R.M.; Direct Determination of Equilibrium Potentials for Hydrogen Oxidation/Production by Open Circuit Potential Measurements in Acetonitrile *Inorg. Chem*. 2013, 52, 3823−3835.

[21] Kolthoff, I.M.; Chantooni, M.K.; Transfer Activity Coefficients of Ortho-Substituted and Non-Ortho-Su bstituted Benzoates between Water, Methanol, and Polar Aprotic Solvents, *The J. Phys. Chem.*, 1974, 78, No. 8.

[22] Kolthoff, M.; Chantooni, M.K.; Hydrogen-Bond Relations between Homoconjugates and Heteroconjugates of Substituted Benzoic Acids and Benzoates in Acetonitrile. Dissociation Constants of Substituted Benzoic Acids. *J. Amer. Chem. Soc.* 1970, 92, 7025.

[23] Nicholas, K.M.; Boucher-Jacobs, C.; Deoxydehydration of Polyols. *Top Curr. Chem.* 2014, 353, 163-184.

[24] Galloni, P.; Conte, V.; Floris, B.; A journey into the electrochemistry of vanadium compounds. *Coord. Chem. Rev.* 2015, 301-302, 240-299.

[25] Wieghardt, T.; Preparation and Characterization of Dipicolinatovanadium(V) Complexes. Kinetics and Mechanism of Their Reaction with Hydrogen Peroxide in Acidic Media. *Inorg. Chem.*1978, 17, 57-64.

[26a] Murray, R.; Feldberg, S.; Feldman, B.J.; An Electrochemical Time-of-Flight Experiment. *J. Phys. Chem.* 1987, 91, 6558-6560.

[26b] Thouin, L.; Sella, C.; Amatore, C.; Electrochemical time-of-flight responses at double-band generator-collector devices under pulsed conditions. *J. Electroanal. Chem.* 2006, 593, 194-202.

[26c] Paul, D.; Meier, M.; Moldenhauer, J.; Rapid and Direct Determination of Diffusion Coefficients Using Microelectrode Arrays. *J. Electrochem. Soc.* 2016, 163, H672-678.

[28] Tsierkezos, N.G.; Cyclic Voltammetric Studies of Ferrocene in Nonaqueous Solvents in the Temperature Range from 248.15 to 298.15. *J. Sol. Chem.* 2007, 36, 289-302.

[29] Compton, R.; Rogers, E.; Wang, Y.; The measurement of the diffusion coefficients of ferrocene and ferrocenium and their temperature dependence in acetonitrile using double potential step microdisk electrode chronoamperometry. *J. Electroanal. Chem.* 2010, 648, 15-19.

[30] Cormac O. Laoire, Sanjeev Mukerjee, and K. M. Abraham. *J. Phys. Chem.* 2009, 113, 20127–20134.

[31] Gonzalez, F.J.; Valencia, D.P.; Understanding the linear correlation between diffusion coefficient and molecular weight. A model to estimate diffusion coefficients in acetonitrile solutions. *Electrochem. Comm.* 2011, 13, 129-132.

Appendix

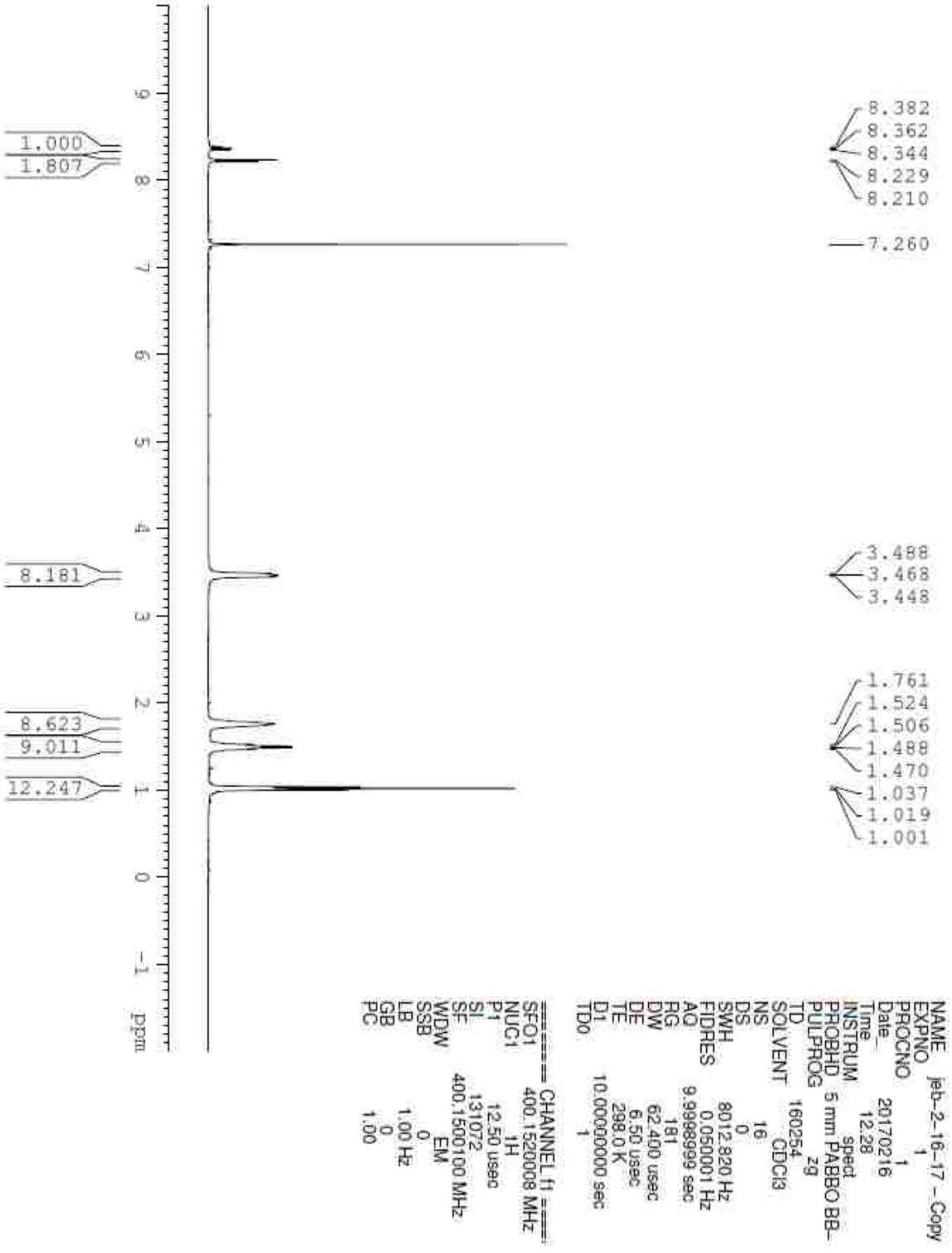

[1]HNMR Spectrum of Tetrabutylammonium dioxovanadiumdipicolinate (TBADVP)

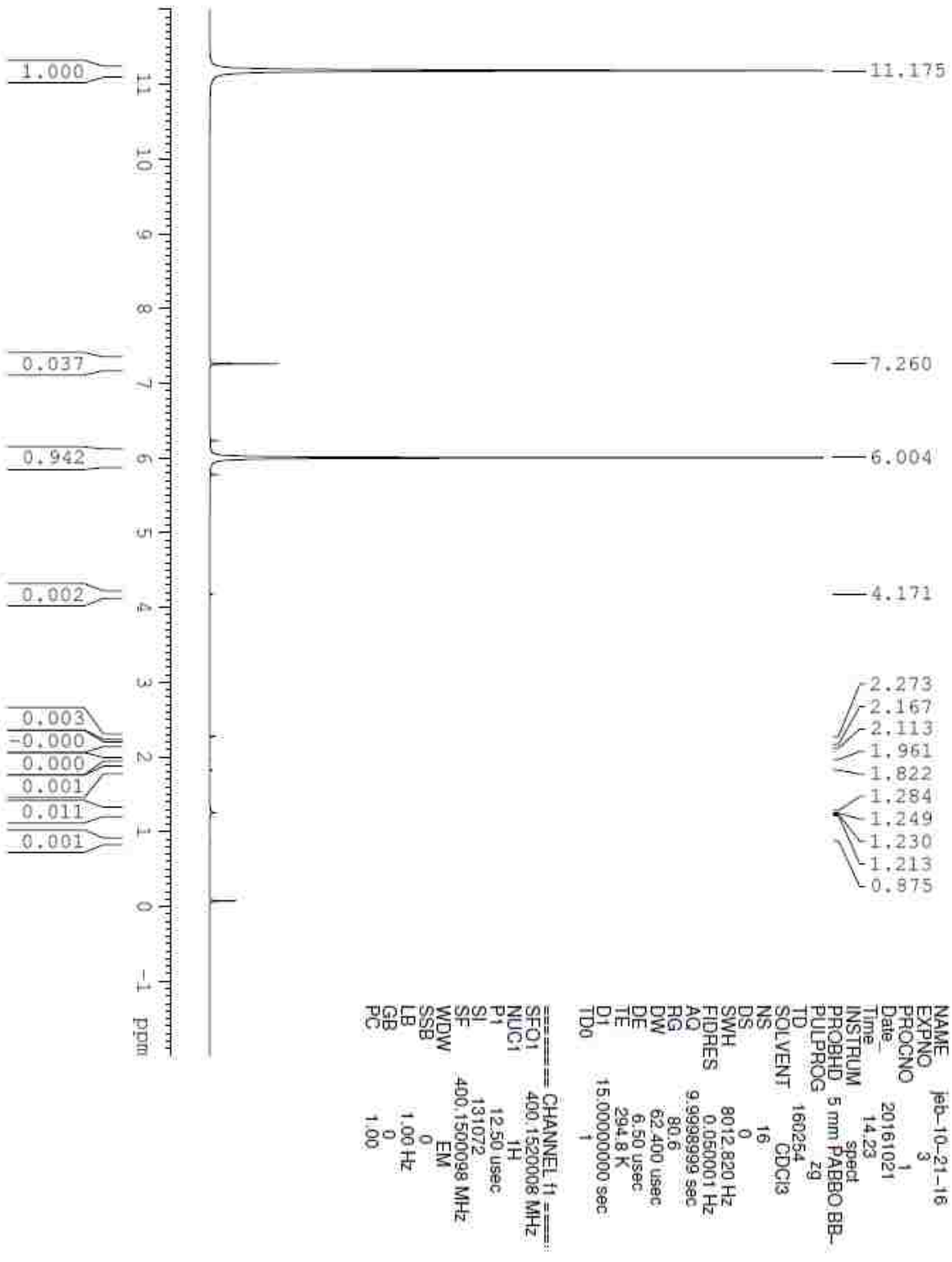

[1]HNMR Spectrum of Dichloroacetic Acid

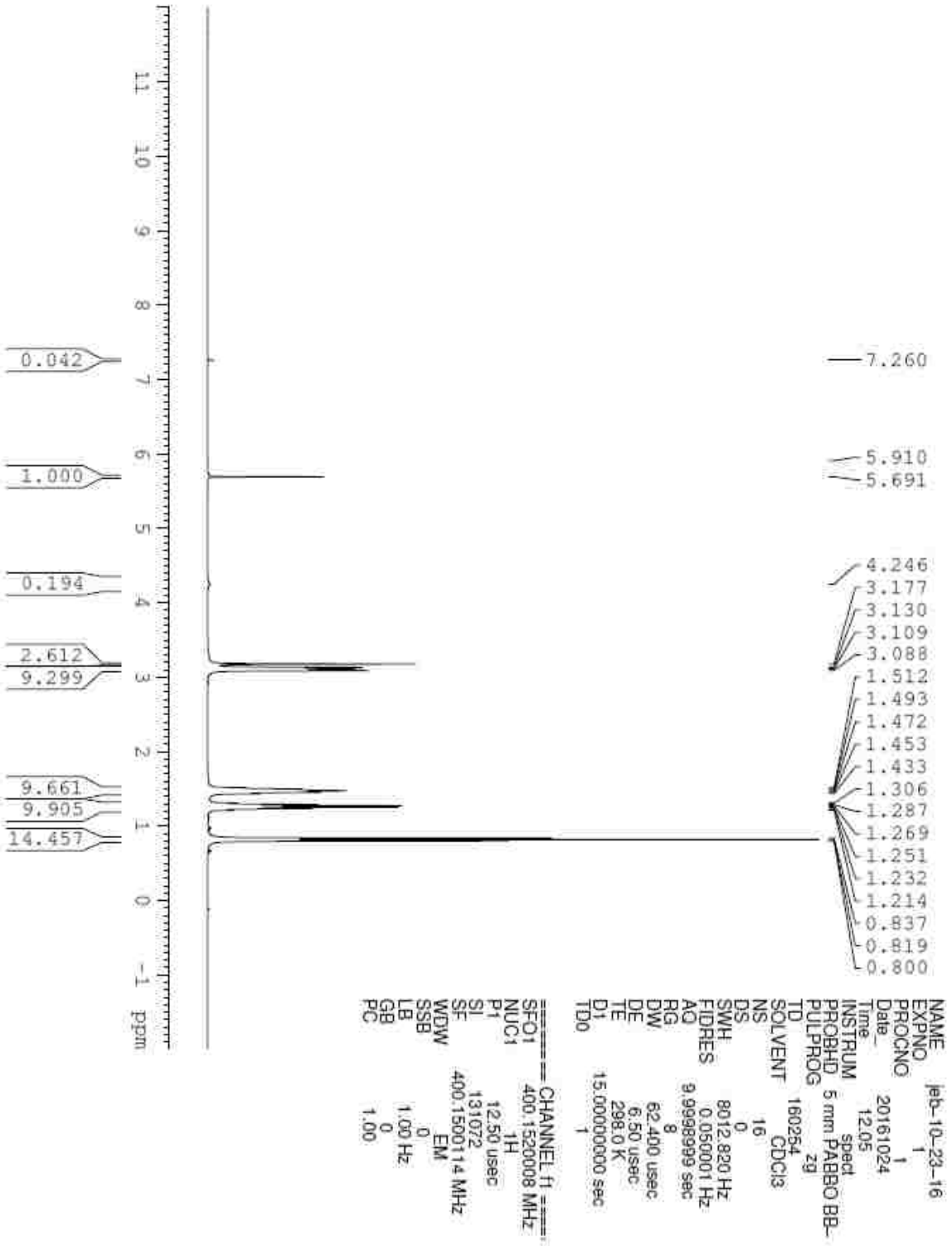

[1]HNMR Spectrum of [n-Bu_4N][dichloroacetate]

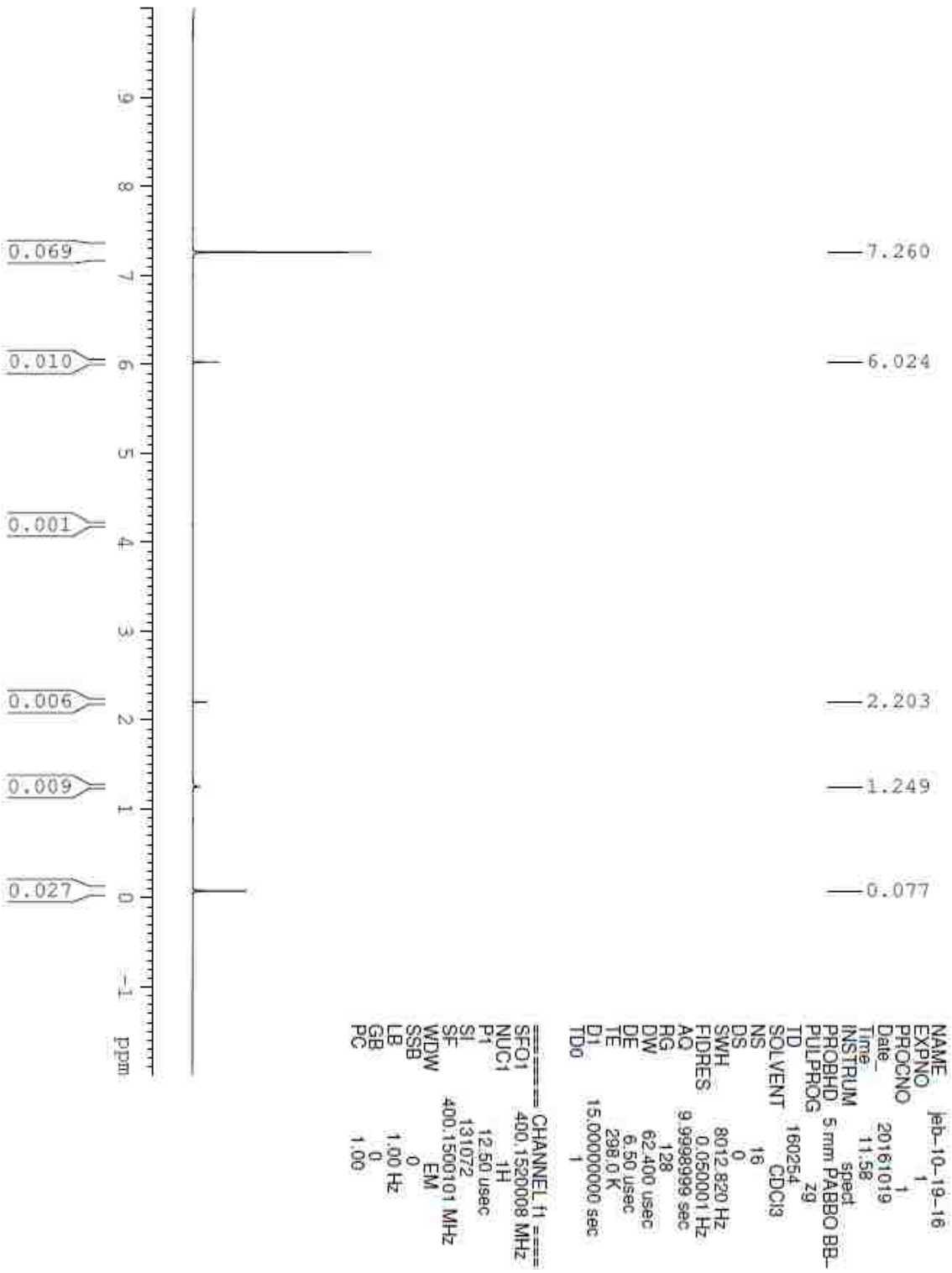

[1]HNMR Spectrum of Trichloroacetic Acid

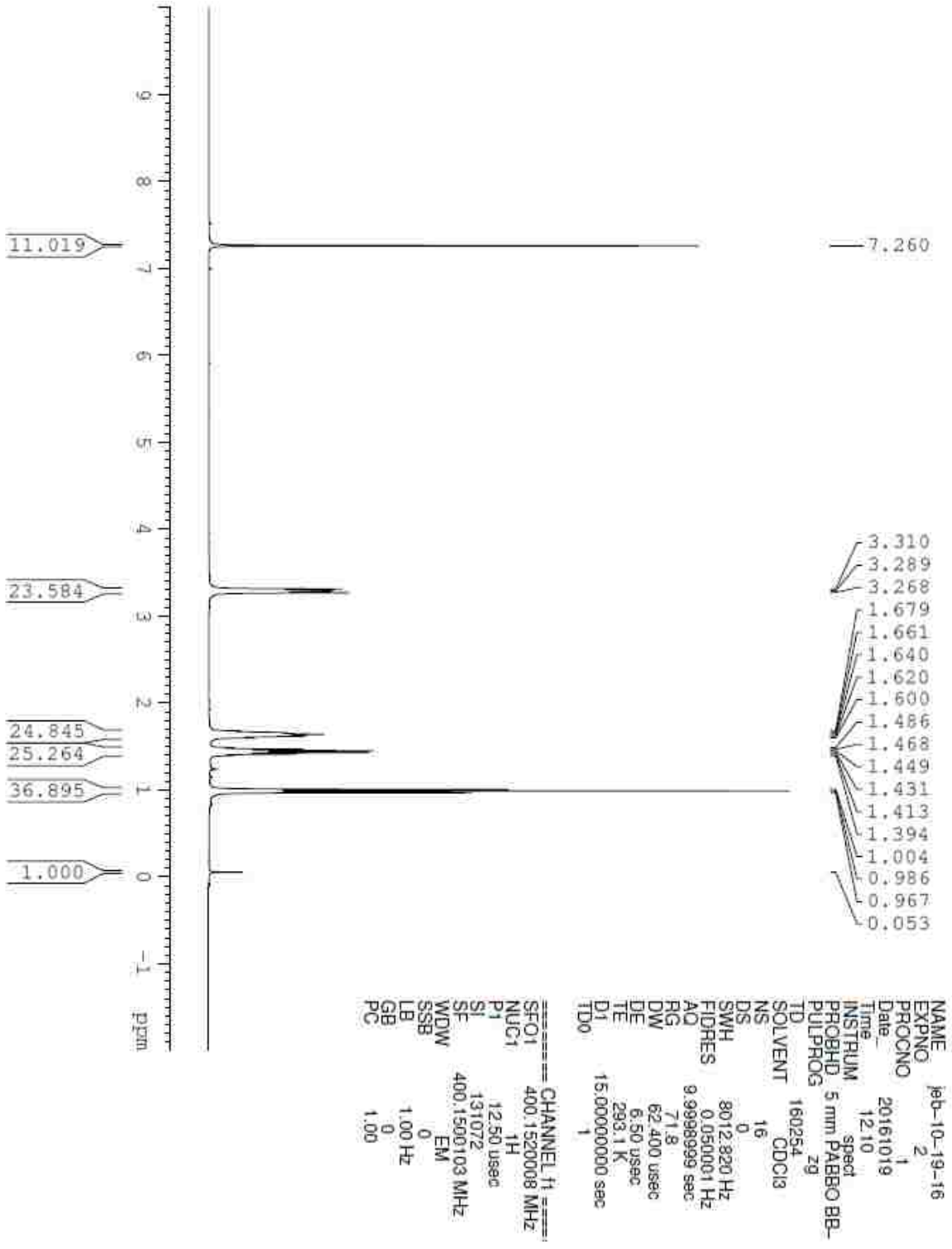

^{1}HNMR Spectrum of [n-Bu_4N][trichloroacetate]

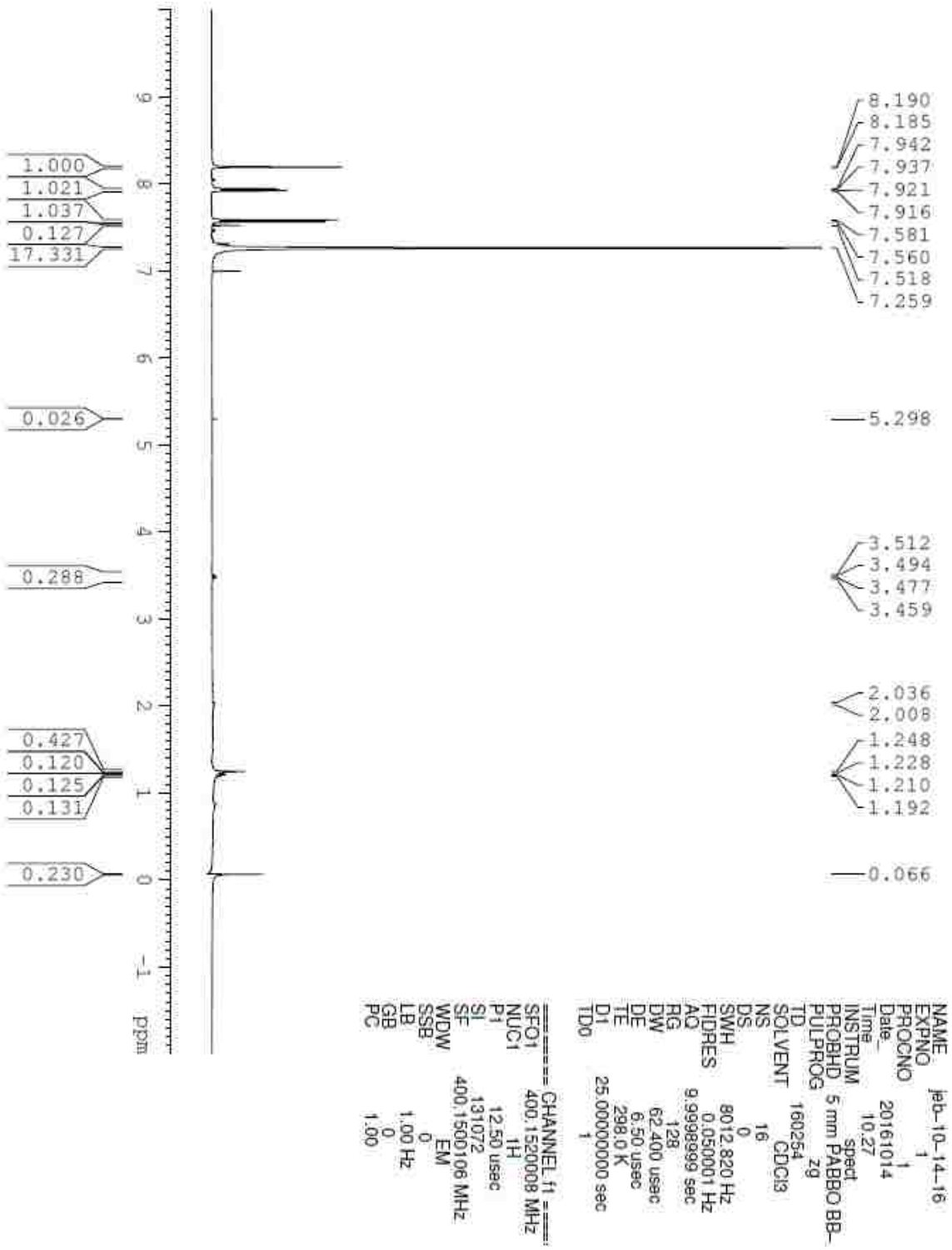

[1]HNMR Spectrum of 3,4-dichlorobenzoic Acid

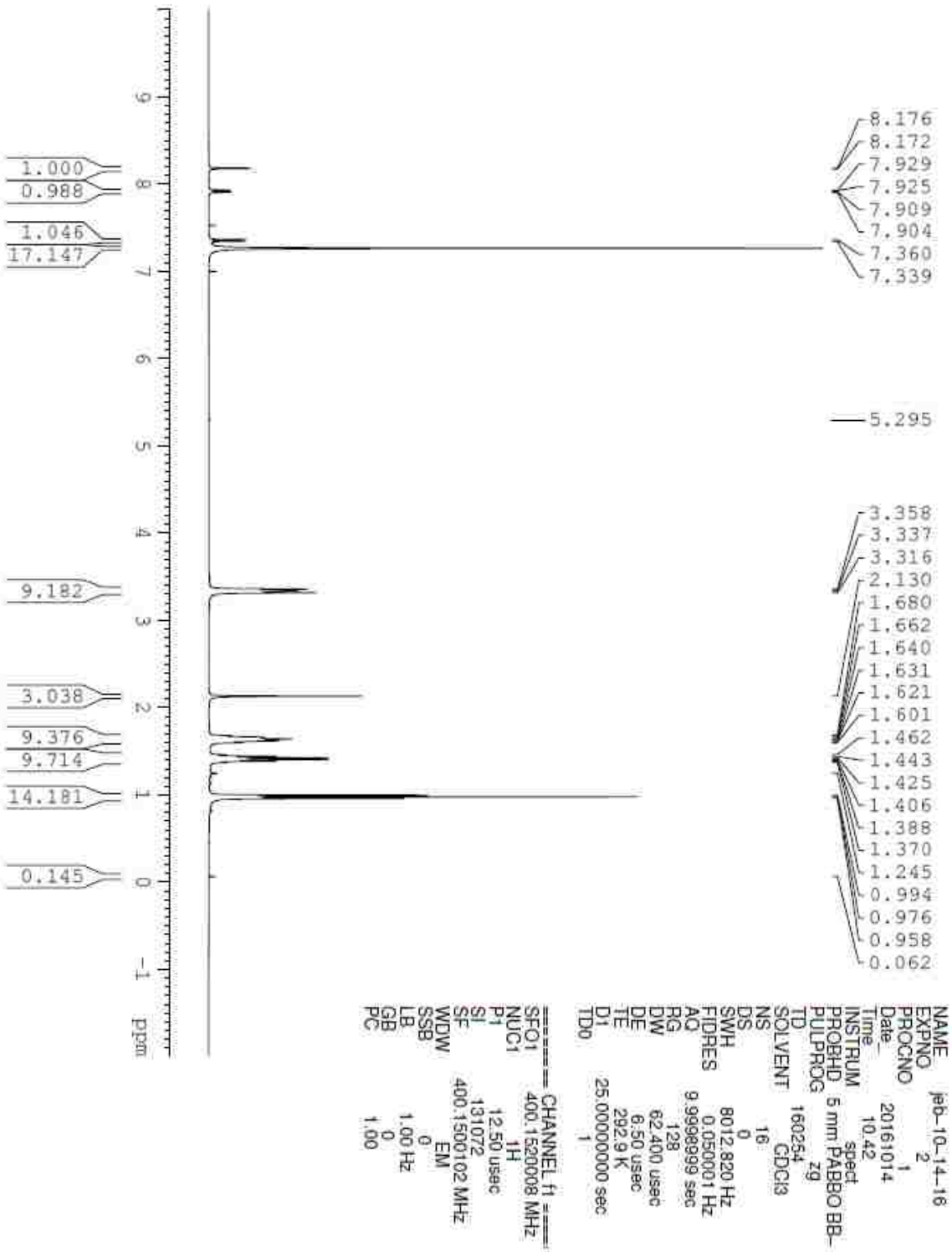

^{1}HNMR Spectrum of [n-Bu_4N][3,4-dichlorbenzoate]

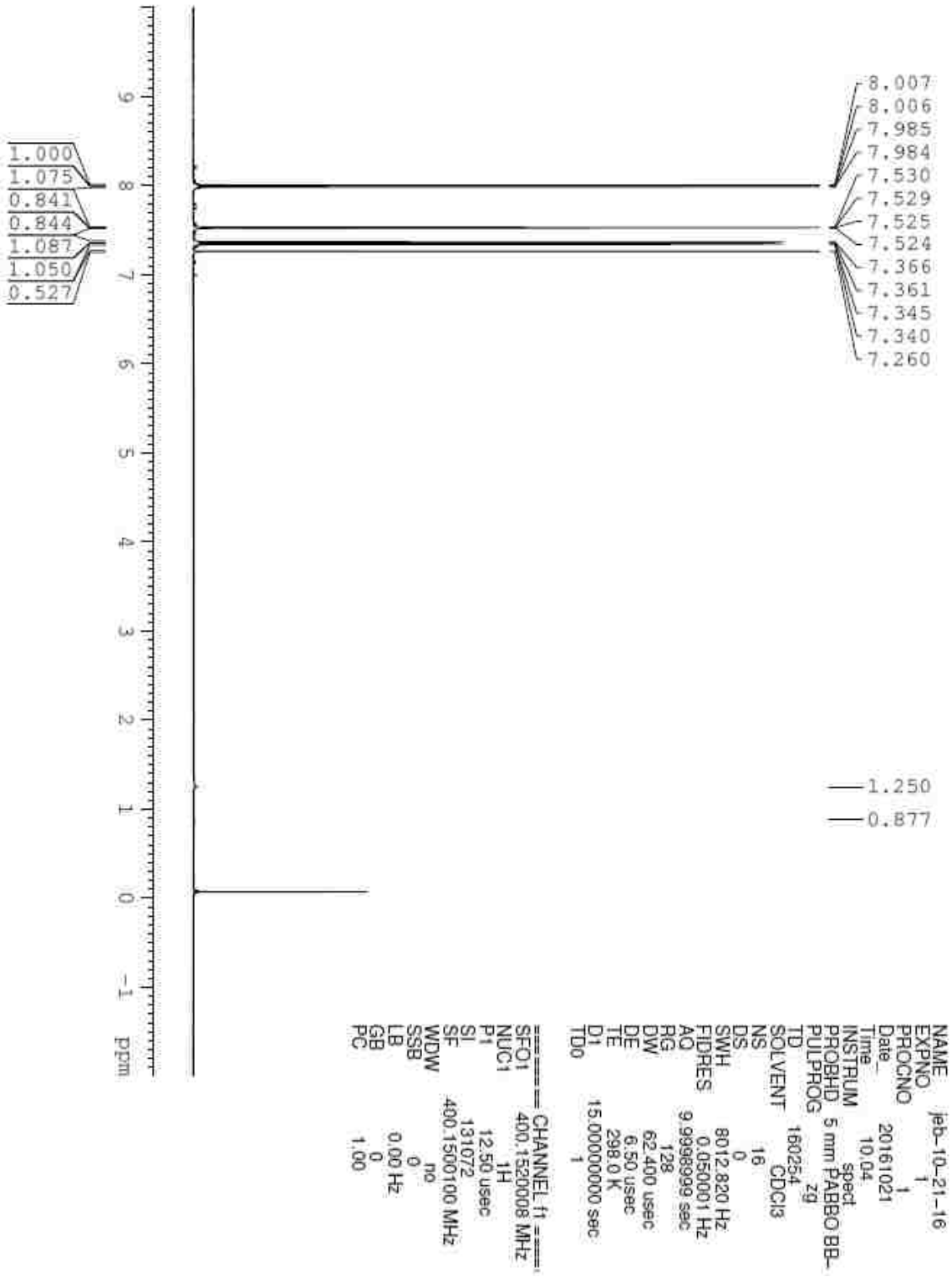

[1]HNMR Spectrum of 2,4-dichlorobenzoic Acid

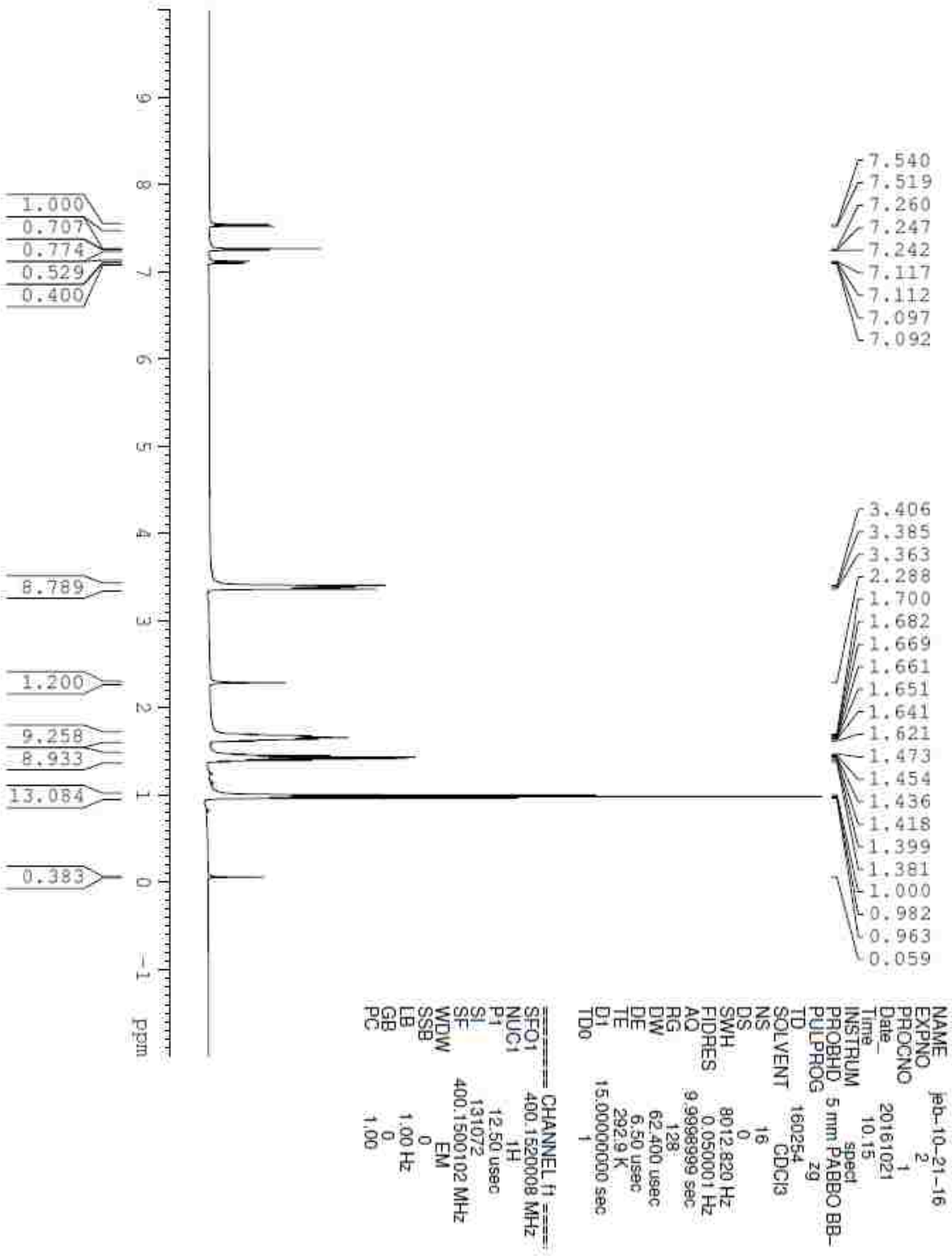

^{1}HNMR Spectrum of [n-Bu_4N][2,4-dichlorbenzoate]

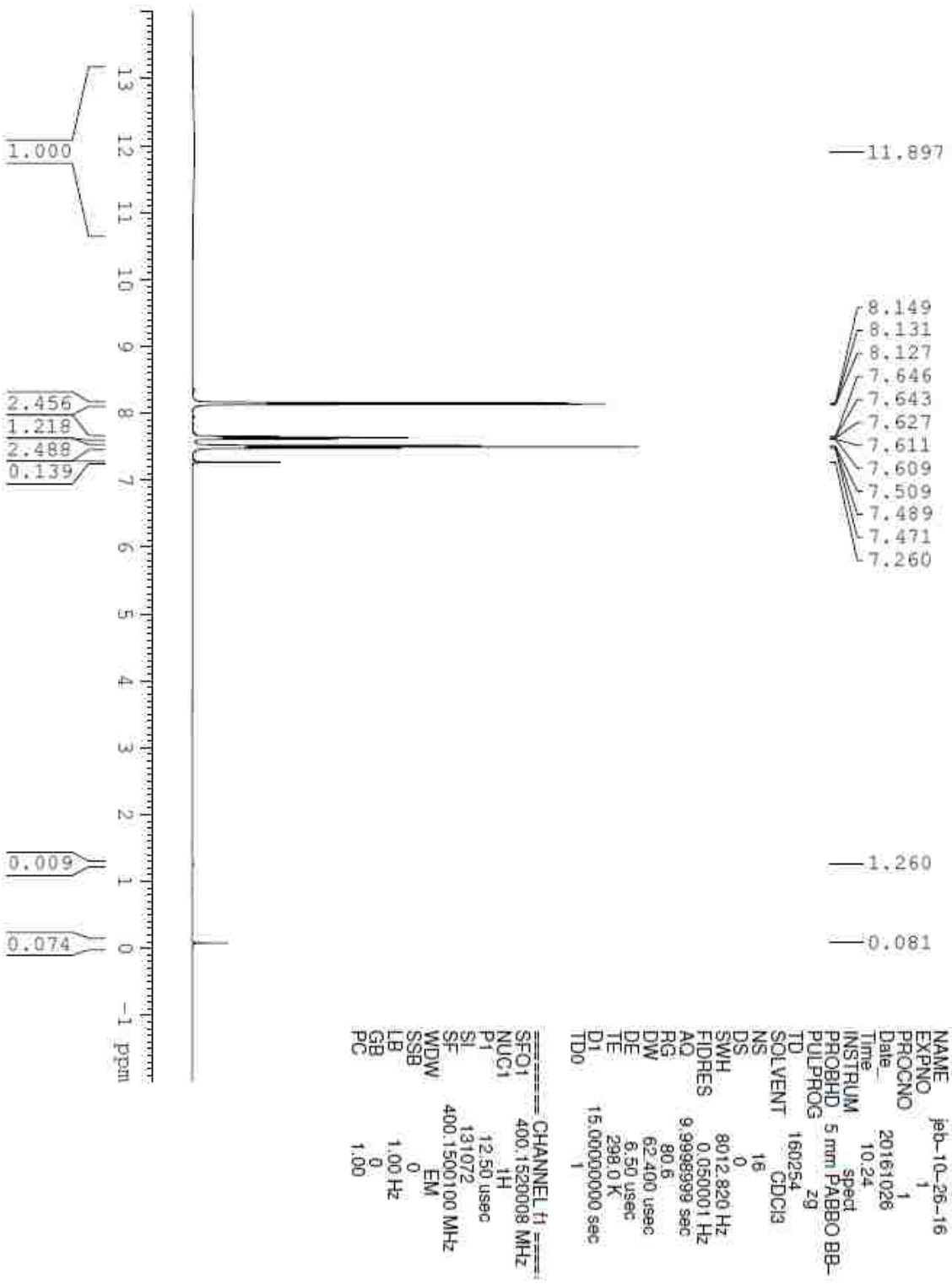

[1]HNMR Spectrum of Benzoic Acid

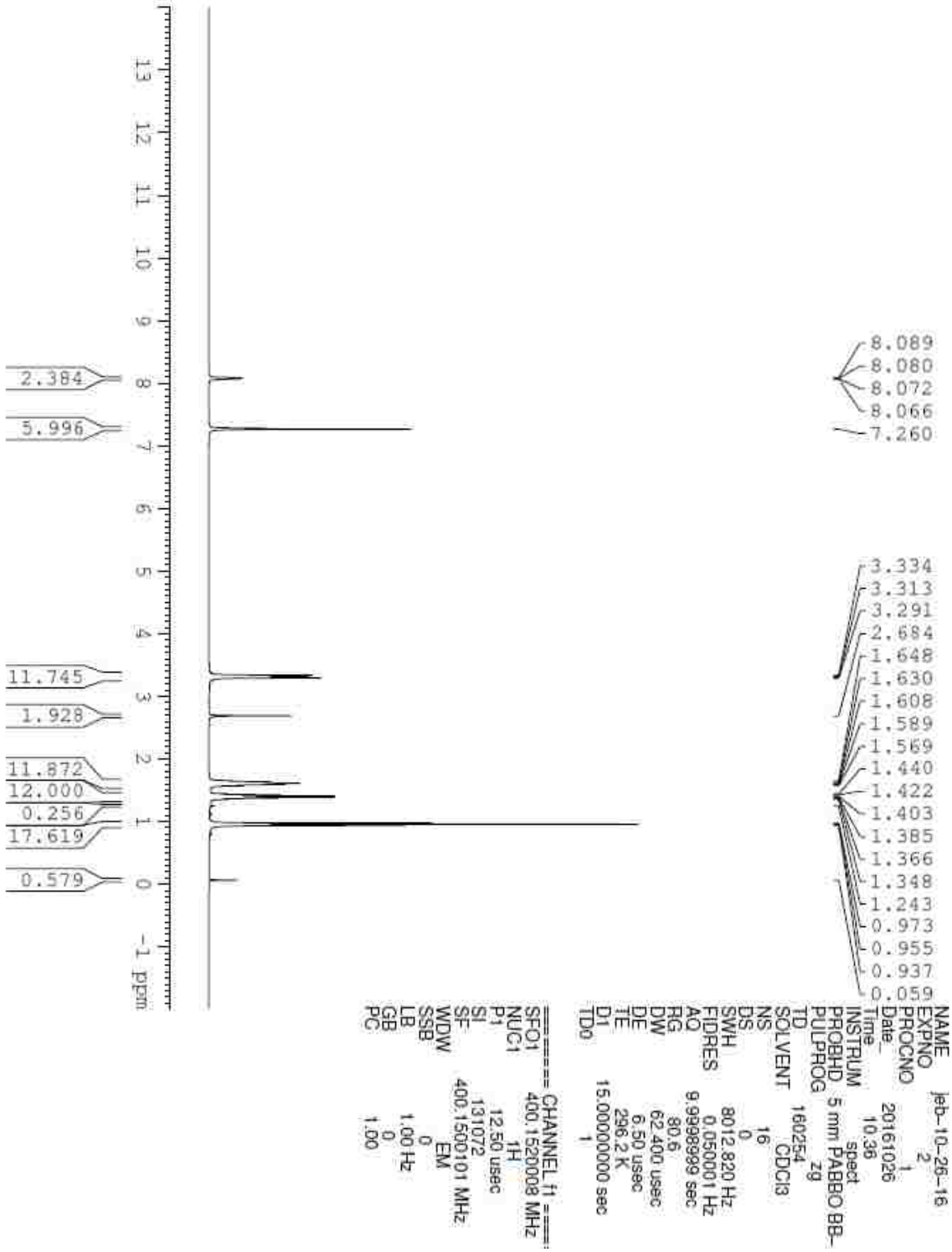

^{1}HNMR Spectrum of [n-Bu_4N][benzoate]

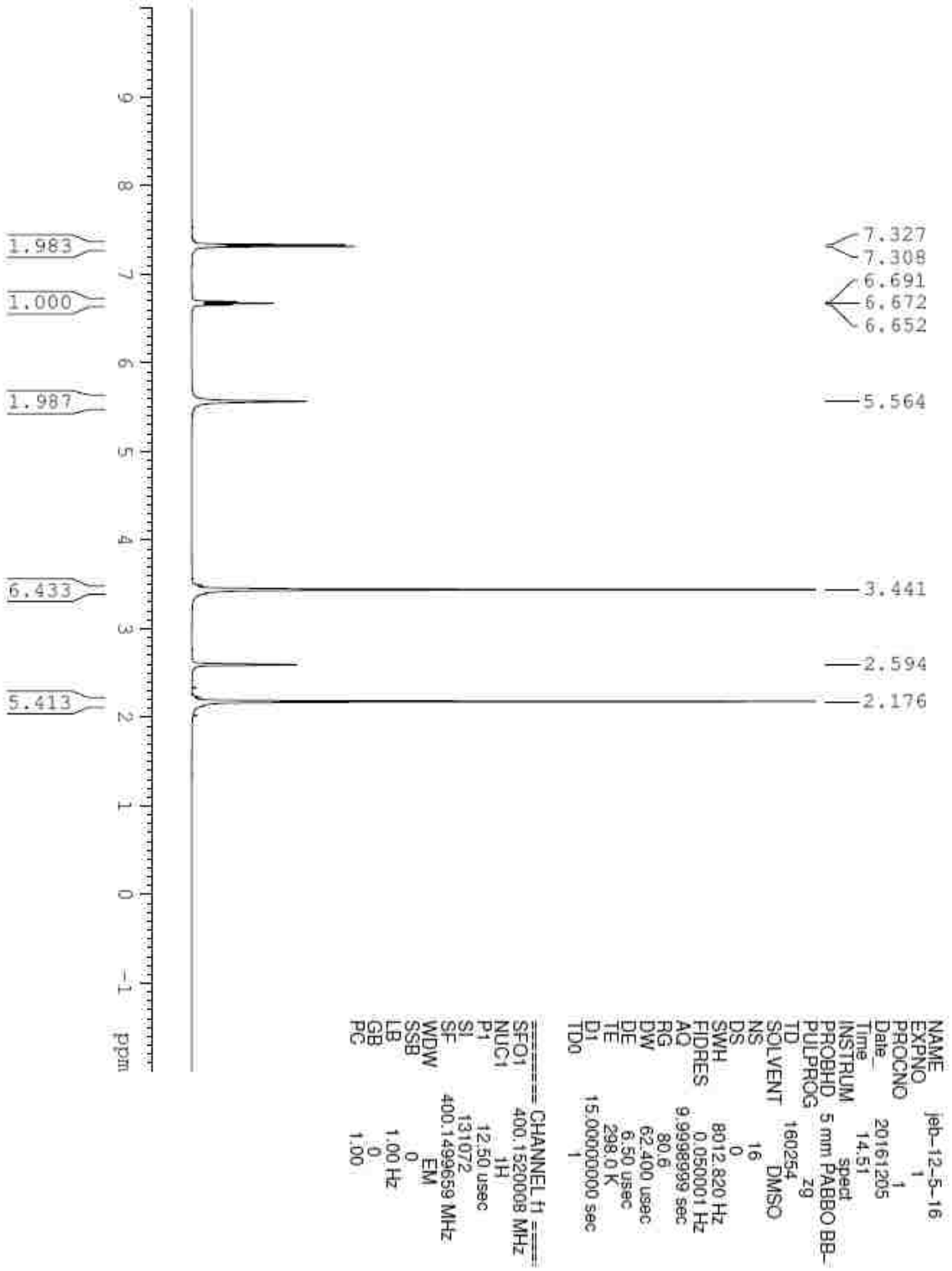

[1]HNMR Spectrum of 2,6-dichloroaniline (sublimed)

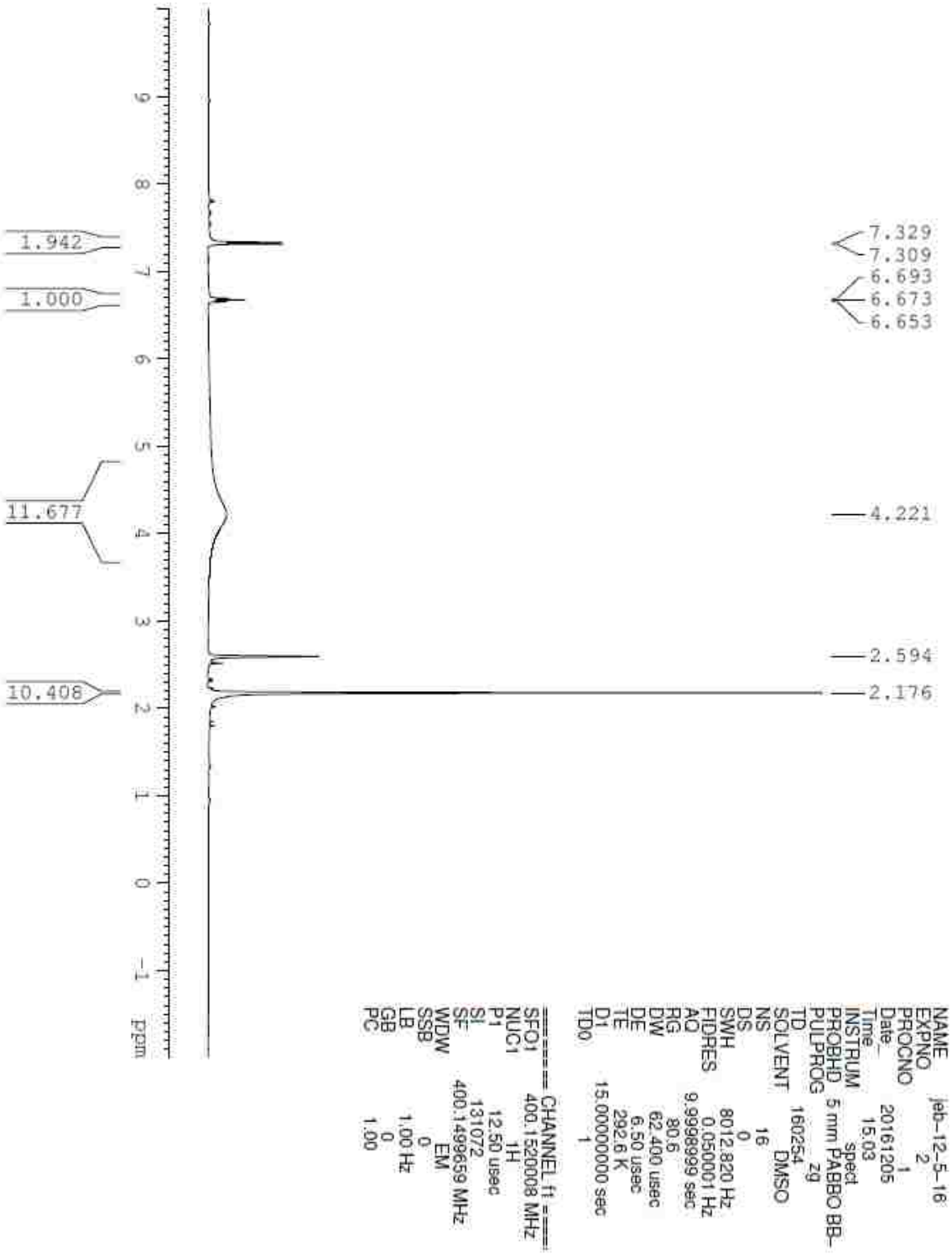

[1]HNMR Spectrum of [TBA][2,6-dichloroanilinium] (sublimed)

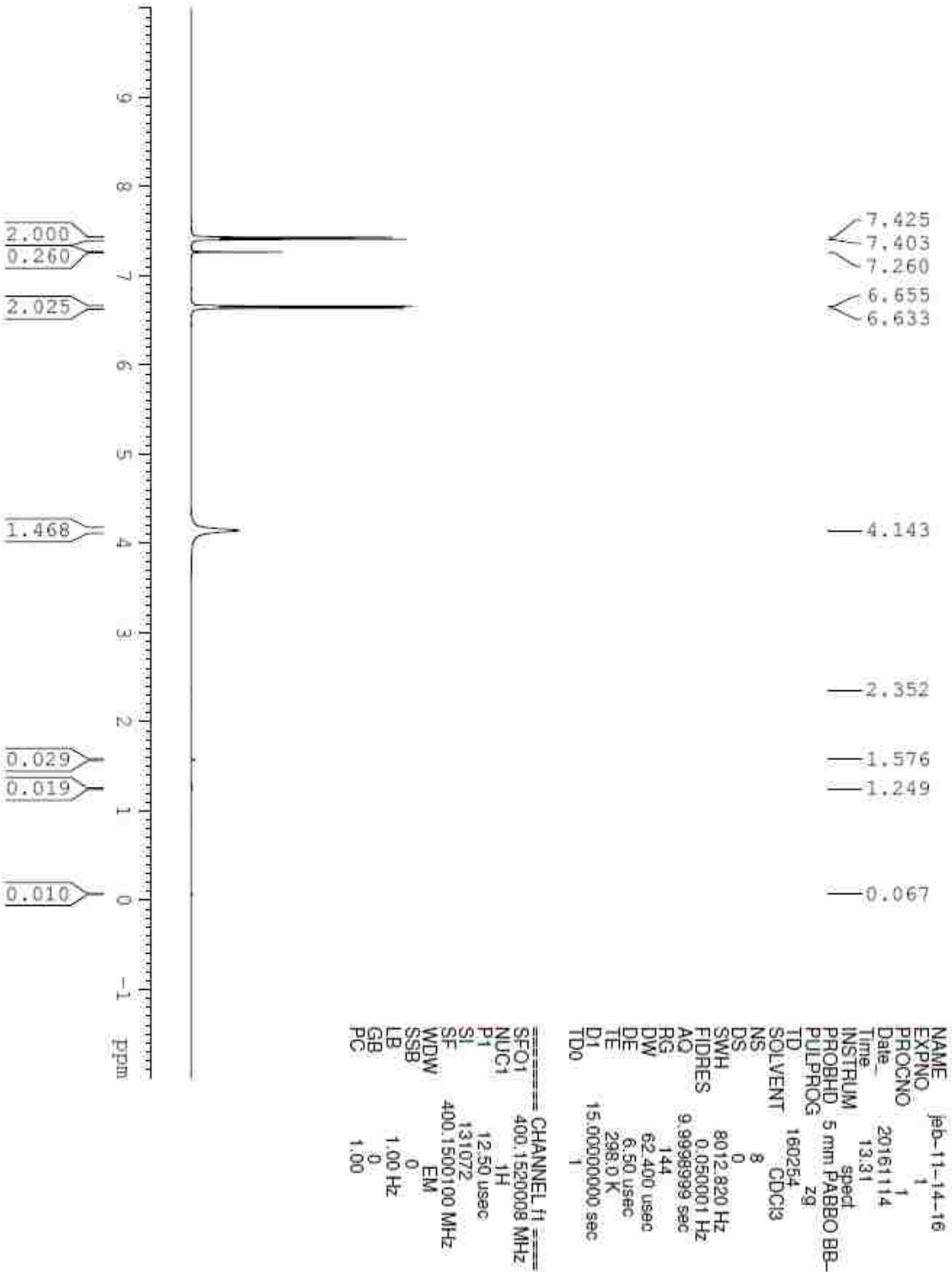

[1]HNMR Spectrum of 4-aminobenzonitrile

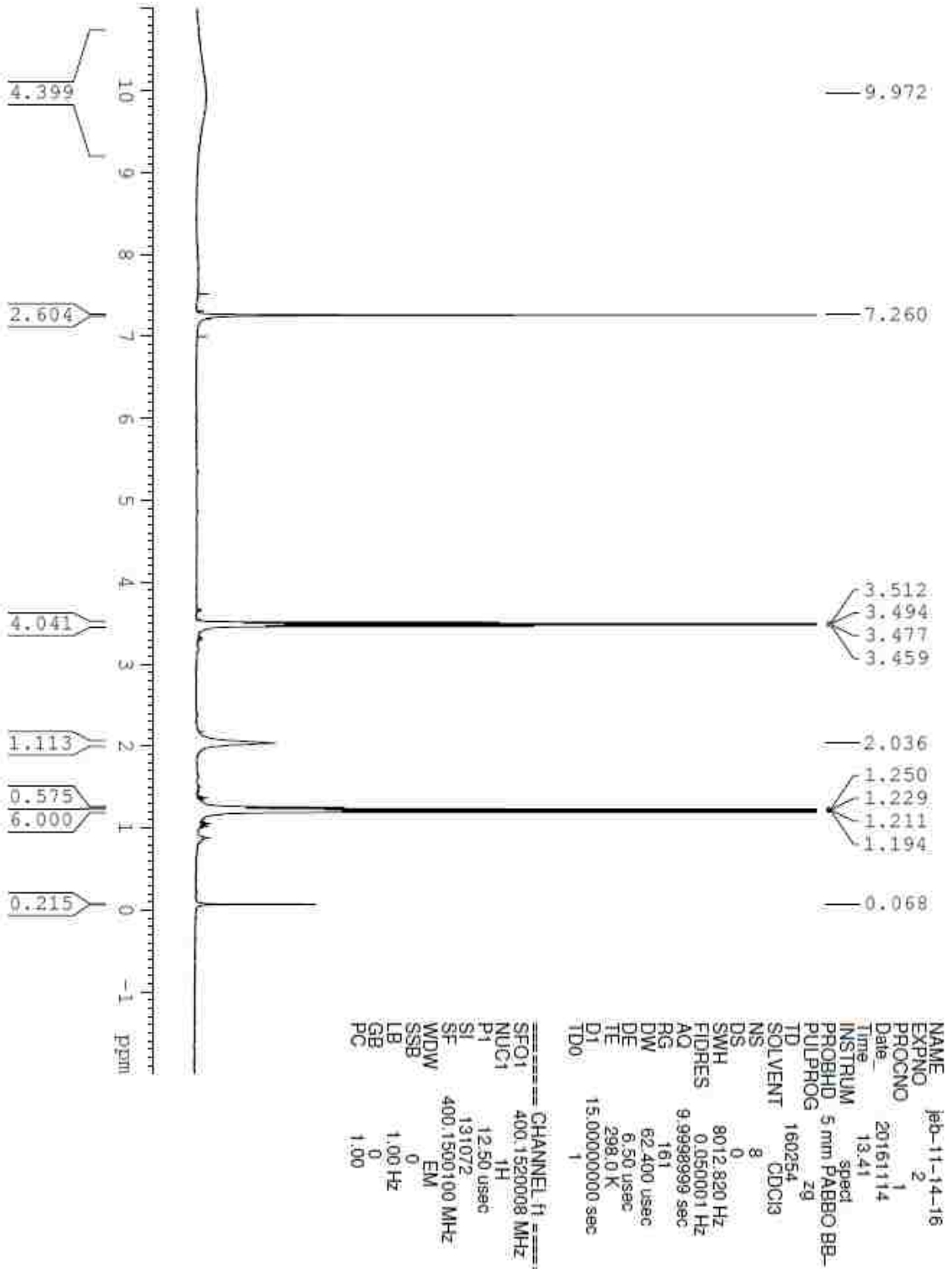

[4-cyanoanilinium][PF_6]